1   **Geographic, seasonal and ontogenetic variations of δ^{15}N and δ^{13}C of Japanese**
2   **sardine explained by baseline variations and diverse fish movements**
3
4   **Authors**
5   Tatsuya Sakamoto[1*], Taketoshi Kodama[2], Sachiko Horii[1], Kazutaka Takahashi[2], Atsushi
6   Tawa[3], Yosuke Tanaka[3], Seiji Ohshmio[1]
7
8   1. Fisheries Resources Institute, Nagasaki Field Station, Japan Fisheries Research and
9   Education Agency, Nagasaki, Japan
10   2. Graduate School of Agricultural and Life Sciences, The University of Tokyo, Tokyo,
11   Japan
12   3. Fisheries Resources Institute, Yokohama Field Station, Japan Fisheries Research and
13   Education Agency, Yokohama, Japan
14
15   *Corresponding author
16   Email: tatsfish@gmail.com
17   Present address: Instituto Português do Mar e da Atmosfera (IPMA), Rua Alfredo
18   Magalhães Ramalho, 6, 1495-006 Lisbon, Portugal
19
20   **Abstract**
21   Understanding and predicting variability in the stable isotope ratios of nitrogen and
22   carbon (δ^{15}N and δ^{13}C, respectively) of small pelagic fish is crucial to enable isotopic
23   studies of a variety of marine predators that feed on them. However, because the isotope
24   ratios reflect plastic feeding habits and fish migration in addition to baseline variation,
25   their predictions require a mechanistic understanding of how each factor contributes. Here,
26   we investigated the habitat-wide variability of δ^{15}N and δ^{13}C of the Japanese sardine
27   *Sardinops melanostictus* in the western North Pacific and its marginal seas (the East China
28   Sea and the Sea of Japan). By combining this with the archived particulate organic matter
29   (POM) dataset as a baseline, we aimed to understand how ecological processes and
30   baseline fluctuations affect isotope ratios of the sardine. Both δ^{15}N and δ^{13}C of sardine
31   showed significant geographical and seasonal trends, with higher values in southern
32   nearshore areas, including the Seto Inland Sea, intermediate values in marginal seas and
33   lower values in Pacific offshore areas. As the variations were largely consistent with the
34   geographic and temporally integrated seasonal trends of isotope ratios of POM,
35   respectively, the baseline variations are the main determinant of sardine isotope
36   composition. The trophic levels of sardine are therefore not significantly different

37 between regions, with possible minor increases in the southern nearshore area. Adults

38 showed less geographic variation than larvae and juveniles, likely due to slower turnover

39 periods and wider migration ranges. Although larval and juvenile isotope ratios in

40 marginal seas mostly reflected the local baseline, those in the Pacific offshore often

41 reflected the baseline in the neighbouring southern region, suggesting contrasting juvenile

42 movements between regions. Our results suggest that the δ^{15}N and δ^{13}C of Japanese

43 sardine strongly reflect baseline variations, but can also be influenced by life-stage- and

44 region-dependent fish movements, thereby demonstrating both the possibility and

45 difficulty of mechanistically modelling the isoscapes of lower trophic level species.

46

47

50

51

52 **Introduction**

53 Stable nitrogen and carbon isotope ratios (δ^{15}N and δ^{13}C, respectively) are an effective

54 tool for studying the migratory behaviours and trophic ecology of marine organisms.

55 Consumer isotope ratios reflect those of prey but have higher values, typically +3.2‰ for

56 δ^{15}N and +1.5‰ for δ^{13}C in fish (Sweetings, 2007a, b; Canseco et al., 2022), due to the

57 preferential uptake of heavier isotopes (DeNiro and Epstein, 1981; Minagawa and Wada,

58 1984). Furthermore, δ^{15}N and δ^{13}C baselines at the lower end of trophic structure, such

59 as marine phytoplankton, exhibit considerable spatial and temporal variation depending

60 on oceanographic conditions (e.g., Kurle and McWhorter 2017; Ho et al., 2021). As a

61 result, δ^{15}N and δ^{13}C of marine organisms can vary depending on diet and habitat,

62 providing valuable insights into the trophic and migratory ecology of marine organisms

63 (e.g., Harrod et al., 2005; Pethybridge et al., 2018; Trueman et al., 2019; Richards et al.,

64 2020). However, to accurately interpret the isotope values, prior knowledge of variation

65 in isotope values of potential prey is essential. Inference of prey and trophic positions can

66 be easily confounded by internal changes in prey isotope values (Phillips et al., 2014).

67 Movements can only be inferred from comparison with the spatial variability of prey

68 isotope values, i.e. isoscape (e.g., Matsubayashi et al., 2019). Therefore, understanding

69 and predicting isotopic variation in lower trophic level species that have a large biomass

70 and are fed on by various predators is of particular importance for the development of

71 isotopic studies in the ecosystem.

72

73

Small pelagic fishes such as sardines (*Sardinops, Sardina* spp.) and anchovies (*Engraulis* spp.) play a key role in the transfer of energy from plankton to higher trophic levels in pelagic ecosystems (Curry et al., 2000; 2011; Kodama et al., 2022a). They inhabit the eastern and western boundaries of subtropical oceans worldwide, including the productive coastal upwelling regions and the western North Pacific, and often dominate zooplankton feeders with their enormous biomass (Checkley et al., 2017). As they are also important prey for a variety of mammals, seabirds and large fishes, and are strongly involved in the trophic pathway to predators (Curry et al., 2000; 2011), understanding the variability of their stable isotope ratios can facilitate ecological studies for various species (e.g., Bode et al., 2003; 2007; 2018; Cardona et al., 2015). Because they feed primarily on plankton, their isotope ratios can be strongly influenced by variations of baseline, which primarily reflect the isotopic signature of primary producers, phytoplankton. However, recent studies show that small pelagic fish, particularly sardines, can exhibit considerable plasticity in their diet, ranging from phytoplankton to fish larvae and eggs, depending on the region and seasons (Costalago et al., 2015). They can also migrate over long distances, even against the Agulhas Current, one of the strongest currents on Earth (Teske et al., 2021). These ecological processes, along with differential turnover rates between trophic levels (Jennings et al., 2008) and potential variation in fractionation factors between prey and consumers (Canseco et al., 2022), may have significant impacts on fish isotope ratios and challenge predictions of the isoscape of small pelagic fish.

94

95

In the western North Pacific and its marginal seas (East China Sea and Sea of Japan), where more than 20 million tonnes of fish are caught annually (FAO, 2021), the most dominant small pelagic fish is the Japanese sardine *Sardinops melanostictus*. Due to its wide habitat and the increase in its biomass since the 2010s (Furuichi et al., 2022), the sardine is becoming increasingly important as prey for marine predators in the western North Pacific (e.g., sei whales *Balaenoptera borealis*, Takahashi et al., 2022), although the knowledge of the δ^{15}N and δ^{13}C dynamics of the Japanese sardine is limited to the local scale (East China Sea and Sea of Japan; Oshimo et al., 2021; Pacific coastal areas: Lindsay et al., 1998; Yasue et al., 2014; Seto Inland Sea; Yamamoto and Katayama, 2012). The habitat of the Japanese sardine includes regions of variable oceanographic conditions. The predominant feature is the Kuroshio and the Kuroshio Extension, which bring in warm subtropical waters from the south (Fig. 1a). The intrusion of the Kuroshio into the East China Sea is the main origin of the Tsushima Warm Current (Inoue et al., 2021). The

109 eggs and larvae found in the coastal areas around the Kuroshio and the Tsushima Warm
110 Current are dispersed by these warm currents (Fig. 1, Oozeki et al., 2007; Itoh et al., 2009;
111 Furuichi et al., 2020). The Kuroshio-Oyashio Transition Zone between the subarctic and
112 subtropical fronts in the Pacific, which is an important nursery area for juveniles (Niino
113 et al., 2020), is full of quasi-stationary jets and mesoscale eddies and meanders (Yasuda,
114 2003; Isoguchi et al., 2006). Subarctic (or subpolar) fronts in the western North Pacific
115 and the Sea of Japan are also evident (Saito et al., 2002; Moriyasu, 1972). The East China
116 Sea is a broad continental shelf influenced by the Kuroshio intrusion and freshwater
117 discharges from the Changjiang River (Zhou et al., 2019), and the Seto Inland Sea is a
118 shallow, semi-enclosed sea in Japan with significant anthropogenic nutrient inputs,
119 characterised by high primary and secondary production and occasional hypoxia
120 (Takeoka 2002; Nakai et al., 2018).
121
122
123 In such a diverse environment, the sardine can change its feeding habits and movement
124 depending on the region and life stage. Analyses of stomach contents at different sites
125 indicate that larvae and juveniles feed mainly on copepods, with the size of plankton
126 consumed increasing with fish size (Hirai et al., 2017; Okazaki et al., 2019; references in
127 Garrido and van der Lingen, 2014). Phytoplankton are often numerically dominant in the
128 stomachs of adults, although full stomachs are usually occupied by zooplankton
129 (references in Garrido and van der Lingen, 2014). In terms of migrations, juveniles in the
130 western North Pacific are assumed to migrate north towards the subarctic region
131 (Sakamoto et al., 2019; 2022), although the knowledge in other regions is severely limited.
132 Adults are considered to migrate seasonally through habitats, generally northwards in
133 summer to feed and southwards in winter for reproduction (Kuroda, 1991). Nevertheless,
134 population-wide differences in trophic and migratory ecology, and the effects on stable
135 isotope ratios, have not been extensively studied especially in recent years.
136
137
138 Importantly, δ^{15}N and δ^{13}C of phytoplankton in the baseline can also vary considerably
139 in the western North Pacific and its marginal seas. The δ^{15}N of phytoplankton depends on
140 the availability of a nitrogen source, which generally increases under nutrient-poor
141 conditions (Rau et al., 1998), and on the δ^{15}N of the source. The input of sewage and the
142 occurrence of denitrification under hypoxic conditions significantly increase the δ^{15}N of
143 nitrate in seawater (Voss et al., 2001; Costanzo et al., 2001), while nitrates derived from
144 nitrogen fixation have a low δ^{15}N (Liu et al., 1996; Horii et al., 2018). Variations in the

145 δ^{13}C of phytoplankton have been associated with various factors, such as δ^{13}C and
146 concentration of dissolved inorganic carbon, species, growth rate and cell size of
147 phytoplankton (Goericke and Fry 1994; Brutemark et al., 2009). As these factors are
148 directly or indirectly related to physical properties of the water column, such as surface
149 water temperature, mixed layer depth and distance from shore, the isotopic composition
150 of phytoplankton often shows contrasts between seasons, current systems and inshore-
151 offshore areas (Magozzi et al., 2017; St. John Glew et al., 2021). Previous studies have
152 found significant geographical variation in isotope ratios of Japanese anchovy (Tanaka et
153 al., 2008) or of various low trophic level fishes combined (Ohshimo et al., 2019) in the
154 region, indicating significant baseline variations. Moreover, the latitudinal and seasonal
155 changes detected in δ^{15}N of European sardine in the Mediterranean were shown to be
156 mainly driven by baseline variations (Gimenez et al., 2023). In order to robustly
157 investigate the ecology of Japanese sardine, therefore, a sufficiently large dataset of
158 baseline isotope ratios covering the entire habitat is required.
159
160
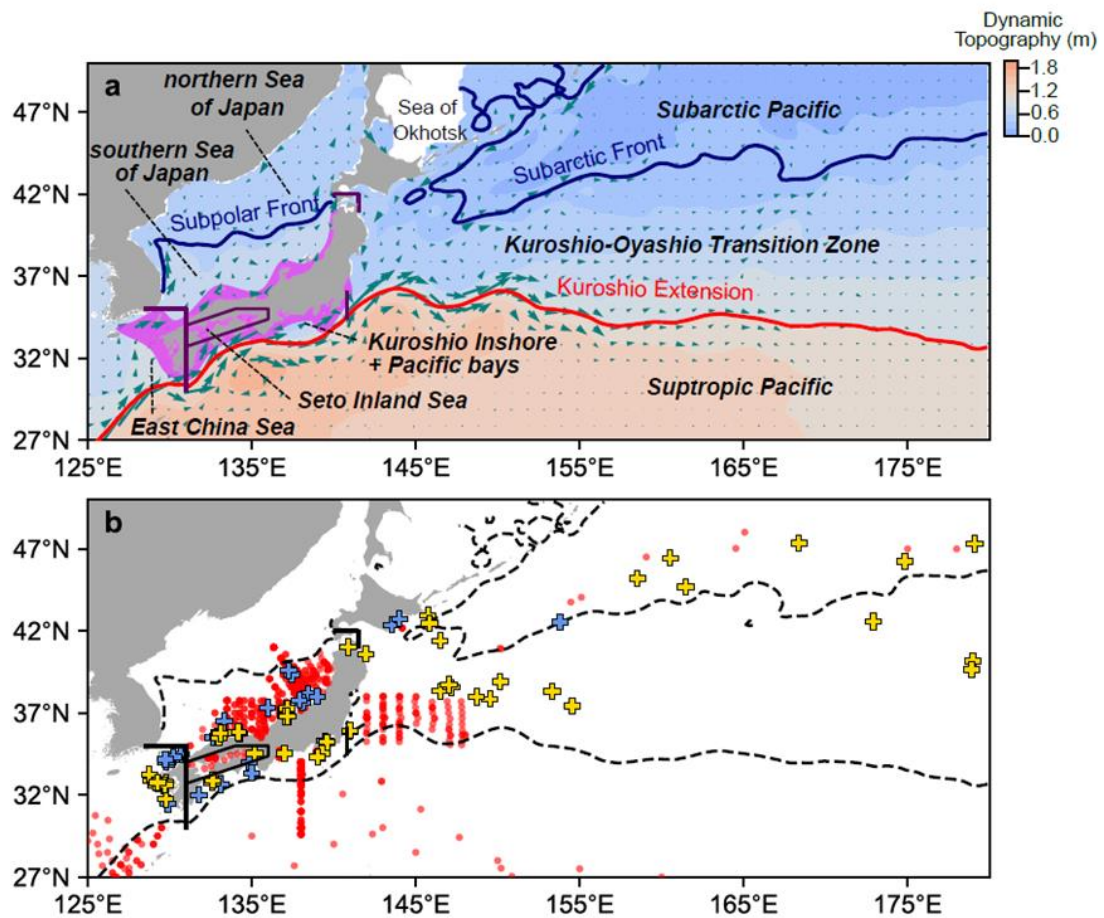
Figure 1. Hydrography around Japanese sardine habitat and sampling locations. Mean absolute dynamic topography (background) during 2001 to 2021 and derived surface geostrophic flow (arrows) are shown with the names of oceanographic provinces (a). Pink shadow: spawning ground of Japanese sardine, red line: 1.05 m contour of dynamic topography corresponding to the Kuroshio and Kuroshio extension axis, Blue lines: 0.55 and 0.30 m contours of dynamic topography corresponding to Subpolar front in the Sea of Japan and subarctic front in the Pacific, respectively (a). Sampling locations of sardine obtained for this study (yellow crosses), sardine from literature (blue crosses) and particulate organic matter (red dots) (b).

In this study, we investigated the geographic, seasonal and ontogenetic variations in δ^{15}N and δ^{13}C of Japanese sardine, to understand variabilities in their migratory and trophic ecology as well as the mechanism of isotopic variation itself. To this end, we have created a comprehensive dataset of sardine isotopic composition by combining newly acquired data with previously published data. By creating an isotopic dataset of particulate organic matter (POM), whose isotope values have often been considered representative of those of the local phytoplankton community (e.g., Goericke and Fry 1994; Kodama et al., 2021), the effects of baseline variation and other ecological processes on sardine isotope ratios

171 were investigated.

172

173

Methods

Sardine sample collection

Larvae, juveniles and adults of Japanese sardine, 300 individuals in total, were collected from samples fished during research surveys and commercial fisheries in 2013 and 2019-2021 (Fig. 1b). Although the collections were not necessarily systematic but rather opportunistic, we aimed to cover the entire distribution of Japanese sardine as much as possible. The main limitation was that we could not collect specimens from the Sea of Okhotsk and the northern part of the Sea of Japan, which are known to be parts of the summer feeding grounds during periods of high biomass (Velikanov, 2016; Muko et al., 2018). The specimens were frozen after landing in commercial fisheries or on board the research vessels and stored at -20 °C until analysis. After thawing in the laboratory, standard length (SL) was measured to the nearest 1 mm and dorsal white muscle tissue was collected for isotopic analysis. To extend data coverage, isotopic values of sardine muscle published in Lindsay et al. (1998), Yasue et al. (2014), Ohshimo et al. (2019, 2021) for a total of 281 individuals were also included in the downstream analyses (Fig. 1b). With the exception of the two larvae in Lindsay et al. (1998), isotope ratios were analysed after lipid extraction. For data where body length was measured in folk length, length was converted to SL using an empirical relationship (Furuichi et al., 2021).

192

193

Stable isotope analysis of sardine muscle

Stable isotope ratios of muscle tissue were analysed according to the method described in previous studies (Ohshimo et al., 2019; 2021). Briefly, tissues were freeze-dried and ground into powder. Lipids were extracted from all samples using a 2:1 chloroform:methanol solution, freeze-dried again and 800 μg of a subsample was extracted for isotope analysis. The δ^{15}N and δ^{13}C values of the samples were determined at Fisheries Resources Institute (Yokohama, Japan) or GeoScience Laboratory (Nagoya, Japan) using a continuous-flow stable isotope ratio mass spectrometer (IsoPrime100, Elementar, Stockton, UK; Delta Plus Advantage, Thermo Fisher Scientific, Waltham, Massachusetts, USA) coupled to an elemental analyser (vario MICRO cube, Elementar; FLASH2000, Thermo Fisher Scientific, Yokohama Japan). The δ^{15}N and δ^{13}C values were reported in δ-notation against the atmospheric N_2 standard and the VPDB reference standard (Vienna Pee Dee Belemnite), respectively, and given as a ‰ value. Analytical

207 accuracies were ± 0.2‰ for $\delta^{15}N$ and $\delta^{13}C$ in both laboratories. The agreement of the
208 reported values between the two laboratories was tested using a blind standard (powder
209 of fish eye lens) where the differences in the reported values for both $\delta^{15}N$ and $\delta^{13}C$ were
210 less than the analytical precisions.
211
212

213 *POM data collection*
214 A meta-analysis was conducted to examine the $\delta^{15}N$ and $\delta^{13}C$ of POM available for the
215 area from 125°E to 180° and 28°N to 50°N, excluding the Yellow Sea in the west of the
216 Korean Peninsula, to cover the areas where sardines were caught. Isotope ratio data from
217 POM that have both $\delta^{15}N$ and $\delta^{13}C$, collected with a glass fiber filter (GF/F) filter in the
218 surface layer (< 50m depth) with known year (since 1990), month and location of
219 sampling, were included in our analyses (Supplementary Table 1). From literature that
220 exhibited data only in its plots, data were extracted from the plots using WebPlotDigitizer
221 (https://automeris.io/WebPlotDigitizer/). The literature data were mainly distributed in
222 the Pacific coasts, the Kuroshio inshore, the Seto Inland Sea and the East China Sea
223 (Minagawa et al., 2001; Takai et al., 2002; 2007; Toyokawa et al., 2003; Wu et al., 2003;
224 Yokoyama and Ishihi, 2003; Kasai et al., 2004; Chen et al., 2006; Hoshika et al., 2006;
225 Yamaguchi et al., 2006; Fukumori et al., 2008; Miller et al., 2010; Sano et al., 2013;
226 Chang et al., 2014; Mino et al., 2016; 2020; Mei, 2018; Ho et al., 2021; Kodama et al.,
227 2021; 2022b; Nakamura et al., 2022). Unpublished isotope data from POM, collected
228 during research surveys conducted by the University of Tokyo and the Japan Fisheries
229 Research and Education Institute in the western North Pacific and its marginal seas during
230 2013–2021, were added to the data set (Supplementary Table 1). During the surveys,
231 seawater samples were collected either by pumping the surface water onboard or by using
232 Niskin bottles in the upper 50m. The collected seawater samples were filtered using a pre-
233 combusted glass fiber filter (GF/F) with a nominal pore size of ~0.7 μm. The filters were
234 frozen on board, thawed and dried in laboratories on land, and then acidified to remove
235 carbonates that could interfere with stable carbon isotope analysis. Stable isotope ratios
236 were measured using either DELTA V advantage-mass spectrometer (Thermo Fisher
237 Scientific Inc), MAT252 (Thermo Fisher Scientific Inc) or Isoprime 100 (Elementer). The
238 $\delta^{15}N$ and $\delta^{13}C$ values were reported in δ-notation against the atmospheric N_2 and VPDB
239 reference standard, respectively, and given as a ‰ value. The analytical precisions were
240 better than ± 0.2‰ for $\delta^{15}N$ and ± 0.2‰ for $\delta^{13}C$.
241
242

243 *Assignments to oceanographic provinces*

244 We divided the western North Pacific and its marginal seas into regions with significantly
245 different water properties based on geography and the positions of the frontal currents,
246 and described the isotopic variations among the regions. The positions of the frontal
247 currents were determined using sea surface level data. Satellite-based, 0.25° × 0.25° sea
248 level dataset "Global Ocean Gridded L4 Sea Surface Heights and Derived Variables
249 Reprocessed" (https://doi.org/10.48670/moi-00148) for 1993–2020 and "Global Ocean
250 Gridded L4 Sea Surface Heights and Derived Variables Reprocessed NRT"
251 (https://doi.org/10.48670/moi-00149) for 2021, both distributed by the Copernicus
252 Marine Environment Monitoring Service, were downloaded from its website
253 (https://resources.marine.copernicus.eu/products). Based on the relationships between
254 current velocity and absolute dynamic topography (ADT) in the Pacific (Nakano et al.,
255 2018) and in the Sea of Japan (Yabe et al., 2021) and visual speculations of the mean
256 absolute dynamic topography (ADT) and geostrophic flow fields during 2001–2021 (Fig.
257 1a), we defined the position of the Subpolar front of the Sea of Japan as ADT = 0.55,
258 Kuroshio and Kuroshio Extension axis as ADT = 1.05, and the subarctic front in the
259 Pacific as ADT = 0.30, around which strong currents were detected (Nakano et al., 2018;
260 Yabe et al., 2021). The ADTs at the sampling points of fish and POM were represented
261 by the monthly mean ADT at the nearest grid point during the year and month of sampling.
262
263

264 All isotopic data from sardine muscle and POM were assigned to one of the nine regions
265 defined as follows (Fig. 1b); (1) Subtropic Pacific; south of the Kuroshio and Kuroshio
266 Extension axis (ADT ≥ 1.05), (2) Kuroshio-Oyashio Transition Zone; north of the
267 Kuroshio Extension axis (ADT < 1.05) and south of the Pacific subarctic front (ADT ≥
268 0.3 or south of 39°N, the condition of 39°N was necessary to distinguish the cold-core
269 rings that often appear in the Kuroshio-Oyashio transition zone (Itoh and Yasuda, 2010)).
270 (3) Subarctic Pacific; north of the Pacific subarctic front (ADT < 0.3 and 39°N), (4) Seto
271 Inland Sea; the inland area north of the Bungo and Kii Channels, (5) Pacific bays; bays
272 facing the Pacific that are generally subject to significant anthropogenic effects (e.g.,
273 Sagami Bay and Ise Bay), automatically detected as less than 10 km from south coast of
274 Japan, (6) Kuroshio inshore; more than 10 km from south coast of Japan and north of the
275 Kuroshio axis (ADT < 1.05), (7) East China Sea: west of 131°E, south of 35°N and north
276 of Kuroshio axis (ADT < 1.05), (8) Southern Sea of Japan: south of the Subpolar front
277 (ADT ≥ 0.55) and (9) Northern Sea of Japan; north of the Subpolar front (ADT < 0.55)
278 in the Sea of Japan.

279

280

281 *Data analysis*

282 To describe the differences in the isotopic composition of sardine and POM between
283 regions and seasons, the δ^{15}N and δ^{13}C values were modelled using linear mixed-effects
284 models. The region factor consists of the nine regions and the season factor of winter
285 (January to March), spring (April to June), summer (July to September) and autumn
286 (October to December) were included as fixed effects. To show the effects of the potential
287 increase in trophic level with growth, the logarithm of fish size (SL) was included as a
288 fixed numerical effect in the model for sardine. This is because the AIC of the models for
289 δ^{15}N and δ^{13}C both decreased by about 10 after the logarithmic conversion from SL. To
290 account for inter-annual variation including the Suess effect on δ^{13}C (Gruber et al., 1999)
291 or the effect on δ^{15}N related to population level of sardine (Bode et al., 2018), the year of
292 sampling was included as a random factor. For the POM isotope ratios, one data point
293 ($\delta15$N: -9.9‰) that fell outside the range of mean $\pm$ 5 standard deviations was excluded
294 from the analysis. In addition, data for which a C:N ratio was available were excluded if
295 the ratio was greater than 10, as this indicates significant inclusion of non-phytoplankton
296 particles (Kodama et al., 2021). When POM was sampled from multiple layers at the same
297 site, the average δ^{15}N and δ^{13}C values of the layers that were less than 50 m deep were
298 considered representative. We used the following model formulae based on the *lmerTest*
299 package (Kuznetsova et al., 2017) in R 4.1.3 (R Core Team, 2022);

300

301 *lmer(Sardine-δ^{15}N or -δ^{13}C ~ region + season + ln(SL) + 1|year)*   (1),

302

303 and

304

305 *lmer(POM-δ^{15}N or -δ^{13}C ~ region + season + 1| year)*   (2).

306

307 The normalities and homogeneities of the residuals were assessed graphically. Fitted
308 parameters of the POM models can be found in Supplementary Tables 2 and 3. Model
309 selections for the fixed effects were performed using the *drop1* function. As dropping a
310 fixed term resulted in significant differences in all cases, the full models were used. The
311 estimated marginal means were calculated for each region and season using the *emmeans*
312 package (Length, 2022) and compared between sardine and POM. For the seasonal means,
313 the 2-season means for POM were also compared with the means for sardine, as seasonal
314 signals in POM are more likely to occur in sardine in a temporally integrated form due to

315   the slower tissue turnover of the fish.

316

317

318   To test for differences in the mean trophic level of sardine between regions, differences
319   in marginal mean δ^{15}N and δ^{13}C between sardine and POM were calculated. The standard
320   errors of the differences were calculated assuming independent error propagation from
321   the marginal means for sardine and POM as follows:

322

323    $(\sigma_{\text{sardine}}{}^2 + \sigma_{\text{POM}}{}^2)^{1/2}$

324

325   where σ_{sardine} and σ_{POM} are the standard errors of marginal means of sardine and POM for
326   each region, respectively, calculated from linear mixed effects models (Formulae 1, 2).
327   Here, the Kuroshio-Oyashio Transition Zone had exceptionally small δ^{15}N difference (see
328   Results). As the low δ^{15}N in larvae and juveniles collected in the Kuroshio-Oyashio
329   Transition Zone during May 2021 had likely contributed to this, the collection sites were
330   compared with mean absolute dynamic topography field and the derived surface
331   geostrophic currents during the survey periods, to investigate potential relationships
332   between local physical dynamics.

333

334

335   *Investigation of short-term movements of larvae and juveniles*
336   If the isotope ratios of a fish are significantly different from the ranges of values that can
337   be predicted from the local baseline of the sampling region, the fish size and the season
338   year of collection, this may indicate that the fish recently came from other regions. Based
339   on this concept, short-term movement patterns of sardine in each region were inferred to
340   clarify the effect of movements on sardine isotope ratios. As the sardine isotope ratios are
341   significantly affected not only by their locations or movements, but also by variations
342   related to fish size, season and inter-annual fluctuations, the observed isotope ratios were
343   first adjusted for these effects to extract the signals from the locations. The adjusted values
344   were calculated by adding the residuals of the mixed effects models (Formula 1) to the
345   marginal means for each sampling region. This is because the residuals are the remaining
346   values after removing the effects of region, fish size, season and inter-annual variation
347   (Formula 1).

348

349

350   Next, the predicted ranges for the adjusted sardine isotope ratios were calculated for each

351 region from the POM isotope ratios. The mean positions of the predicted range for each
352 region were calculated from the marginal mean POM isotope ratios (Supplementary Table
353 4) using the regression of the marginal mean isotope ratios of sardine on those of POM
354 (see Results, Equations 3, 4). Uncertainty ranges were calculated assuming independent
355 propagation of errors in the estimation of marginal means for POM, the mean error in the
356 regression, and individual-level variability due to undescribed causes (e.g., individual
357 preferences of prey size) as follows:

358

359 $(\sigma_{\text{POM}}^2 + RMSE^2 + \sigma_{\text{residual}}^2)^{1/2}$

360

361 where σ_{POM} are the standard errors of marginal means for POM (Supplementary Table 4),
362 $RMSE$ is the root mean square error in regression of sardine mean on POM mean
363 (Equations. 3, 4; 0.42 in δ^{15}N, 0.52 in δ^{13}C), and σ_{residual} is the standard deviation of the
364 residual in the mixed effects model (Formula 1; 1.37 in δ^{15}N, 0.71 in δ^{13}C). For the
365 calculation of $RMSE$, the residual for the Kuroshio-Oyashio Transition Zone were
366 excluded as the sardine isotope ratios there likely do not reflect the baseline there. The
367 predicted ranges in a δ^{13}C-δ^{15}N diagram were defined as ellipses with a width and height
368 equal to twice the uncertainties for δ^{13}C and δ^{15}N, respectively.

369

370

371 The entire habitat was divided into three major areas, namely the marginal seas including
372 the Northern and Southern Sea of Japan and East China Sea, the nearshore area including
373 Seto Island Sea, Pacific bays, Kuroshio inshore, and the Pacific offshore area including
374 the Subtropical and Subarctic Pacific and Kuroshio-Oyashio Transition Zone. In each area,
375 the adjusted sardine isotope ratios were compared with the predicted ranges for each
376 region to infer movement patterns. For the nearshore area, the predicted range for the
377 Subtropical Pacific was also included in the comparison, as individuals can arrive from
378 there via the Kuroshio. We used this procedure only for larvae and juveniles (< 160 mm
379 SL). Given the presumed spawning migration from the Pacific offshore to the Southern
380 nearshore area (Kuroda, 1991) and similar isotope ratios between regions (see Results),
381 it was difficult to assume that the adults remain in each area but allowing too many options
382 that cannot be completely separated would limit the validity.

383

384

Results
386 *Geographical and ontogenetic variations in isotopic composition of sardine*

387   The stable isotope ratio data of 581 individuals, ranging from 21 to 232 mm SL, were
388   available in total. The number of available data varied by regions, ranging from 31 in the
389   Seto Inland Sea to 153 in the Southern Sea of Japan (Supplementary Fig. 1). The δ^{15}N
390   and δ^{13}C values of sardine muscle ranged between +5.4‰ to +16.4 ‰ and -21.2‰ to -
391   14.2 ‰, averaged +9.5 (± 1.8, 1SD) ‰ in δ^{15}N and -18.5 (± 1.1) ‰ in δ^{13}C, and showed
392   a significant positive correlation between them (Pearson's r = 0.74, n =581, p < 10^{-10}).
393   The isotope ratios of larvae and early juveniles (< 60 mm SL based on the definition of
394   Smith (1992)) showed patchy distribution away from the values often seen in late
395   juveniles (60−160 mm SL) or adults (>160 mm SL) (Fig. 2a, b). The values of late
396   juveniles were distributed broadly with geographical variations (Fig. 2c), while values of
397   adults were mostly concentrated around the global mean values (+9.5‰ in δ^{15}N and -
398   18.5‰ in δ^{13}C) or to the highest or lowest extremes (Fig. 2d).
399
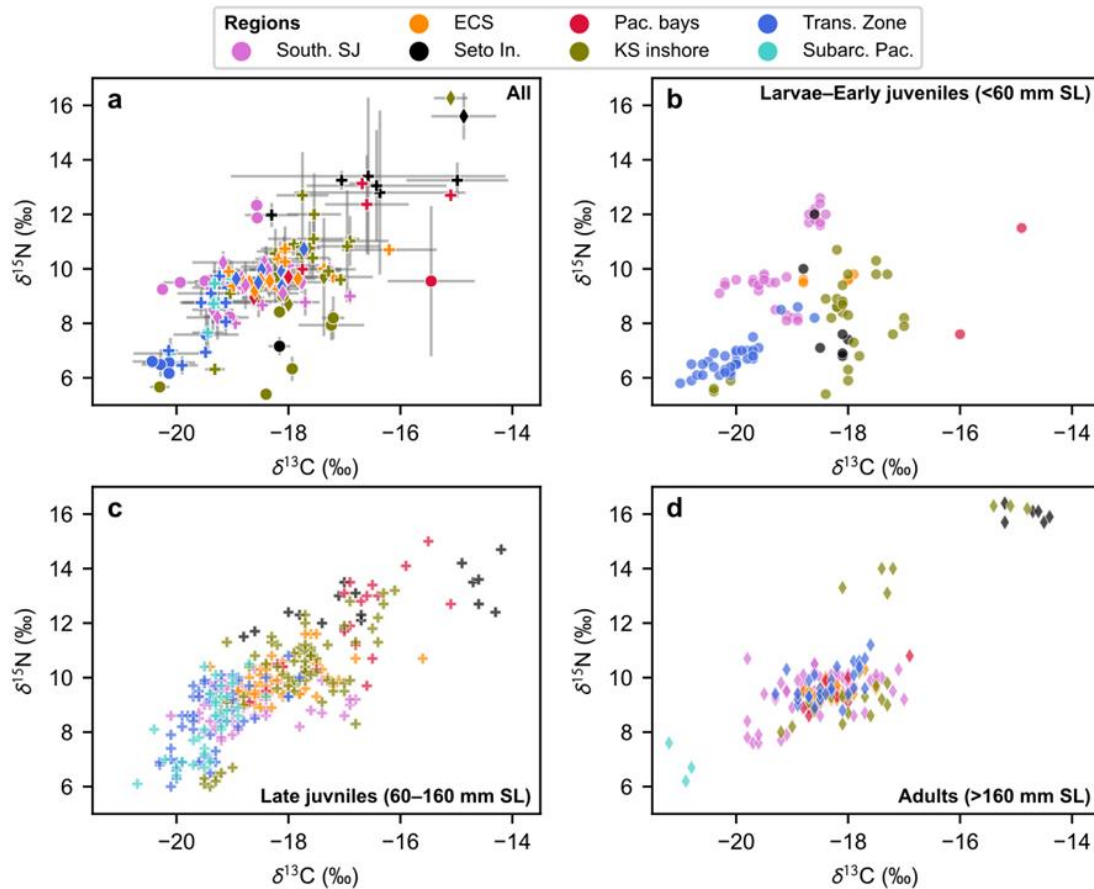
Figure 2. Stable carbon and nitrogen isotope ratios of Japanese sardine. The mean $\delta^{13}C$ and $\delta^{15}N$ of captured in the same location and date are shown with standard deviations, with symbols representing life history stages (circle: larvae and early juveniles, plus mark: late juveniles and diamond: adults) and colors representing sampling regions (a). Data for each individual separately shown for larvae and early juveniles (b), late juveniles (c) and adults (d).

400

401

402 Significant positive correlations were detected between isotope ratios and fish size ($\delta^{15}N$:

403 Pearson's r = 0.30, p = 2.0×10^{-13}, $\delta^{13}C$: r = 0.26, p = 3.6×10^{-10}) or the logarithm of fish

404 size ($\delta^{15}N$: r = 0.32, p = 2.8×10^{-15}, $\delta^{13}C$: r = 0.27, p = 8.3×10^{-11}). However, even excluding

405 adults, which showed less geographical variation (Fig. 2d), the relationships between size

406 and isotope ratios were significantly different between regions (Fig. 3a−f). Relatively

407 limited changes were observed during larval and juvenile stages in the Southern Sea of

408 Japan and the adjacent East China Sea (Fig. 3a, d), although negative correlations between

409 size and $\delta^{15}N$ were observed (Southern Sea of Japan: Spearman's r = -0.35, p = 8.0×10^{-4};

410 East China Sea: r = -0.36, p = 2.2×10^{-3}). Large variations were observed in the Seto Inland

411 Sea, Pacific bays and Kuroshio inshore area (Fig. 3b, e), where remarkably low $\delta^{15}N$ (<

412 +8‰) were observed in some fish under 100 mm SL and high $\delta^{15}N$ (> +12‰) and $\delta^{13}C$

413   (> -17‰) were observed in some larger juveniles (Fig. 3b, e). Positive correlations
414   between size and δ^{15}N were found in the Kuroshio inshore (Spearman's r = 0.59, p =
415   2.7×10^{-10}) and Seto Island Sea (p = 0.62, p =8.4×10^{-4}). Individuals smaller than 100 mm
416   SL in the Kuroshio-Oyashio transition zone tended to show lower δ^{15}N and δ^{13}C than
417   larger individuals in the region, while in the Subarctic Pacific, individuals larger than 130
418   mm SL tended to show lower δ^{15}N and δ^{13}C (Fig. 3c, f). A correlation between size and
419   δ^{15}N for larvae and juveniles was found to be positive in the Transition Zone (Spearman's
420   r = 0.70, p = 6.7×10^{-14}) but not significant in the Subarctic Pacific (r = -0.30, p = 0.07).
421
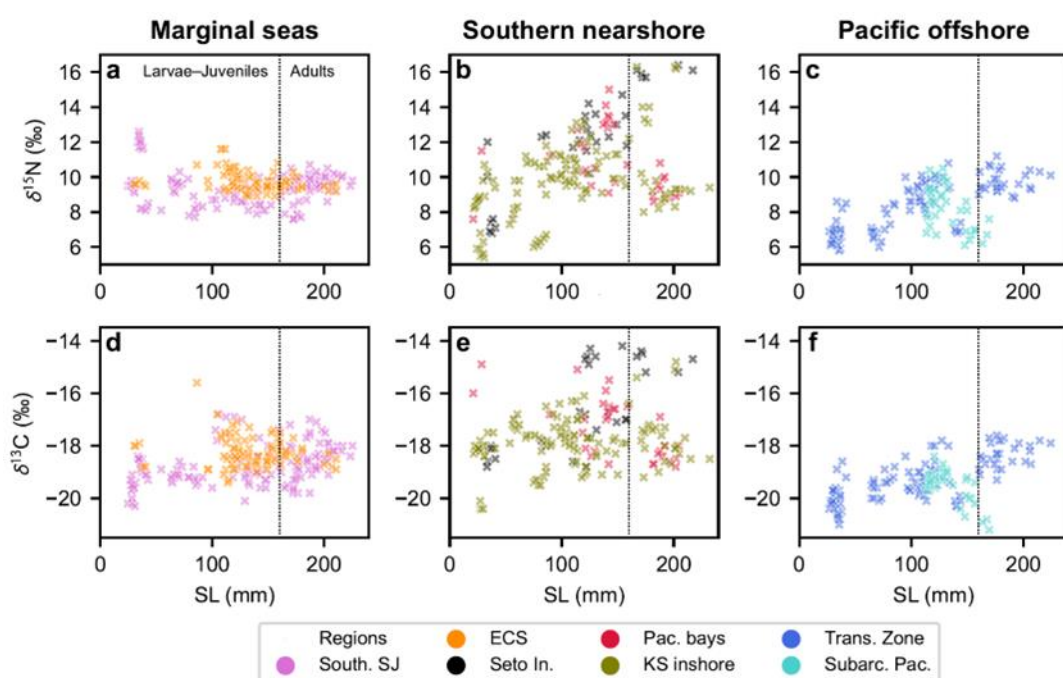
Figure 3. The relationships between isotope ratios and length of sardine. The relationships between δ^{15}N and standard length (SL) (a-c) and δ^{13}C and SL (d-f) for the East China Sea and the Sea of Japan (a, d), Seto Inland Sea and regions off southern coast (b, e) and the Pacific offshore regions (c, f) are shown. Colors represent the regions of sampling.

422

423

424   For all sizes combined, the geographical variations were evident for both δ^{15}N and δ^{13}C
425   (Fig. 4a-b). For both δ^{15}N and δ^{13}C of sardine, medians were higher in the Seto Inland
426   Sea and Pacific bays, moderate in the Kuroshio inshore, East China Sea, Southern Sea of
427   Japan and Sea of Japan Coast, and lower in the Kuroshio-Oyashio Transition Zone and
428   Subarctic Pacific. Seasonal trends were not consistent between regions, although the
429   seasonal median in each region tended to be higher in summer (July to September) and
430   autumn (October to December) (Fig. 4a, b).
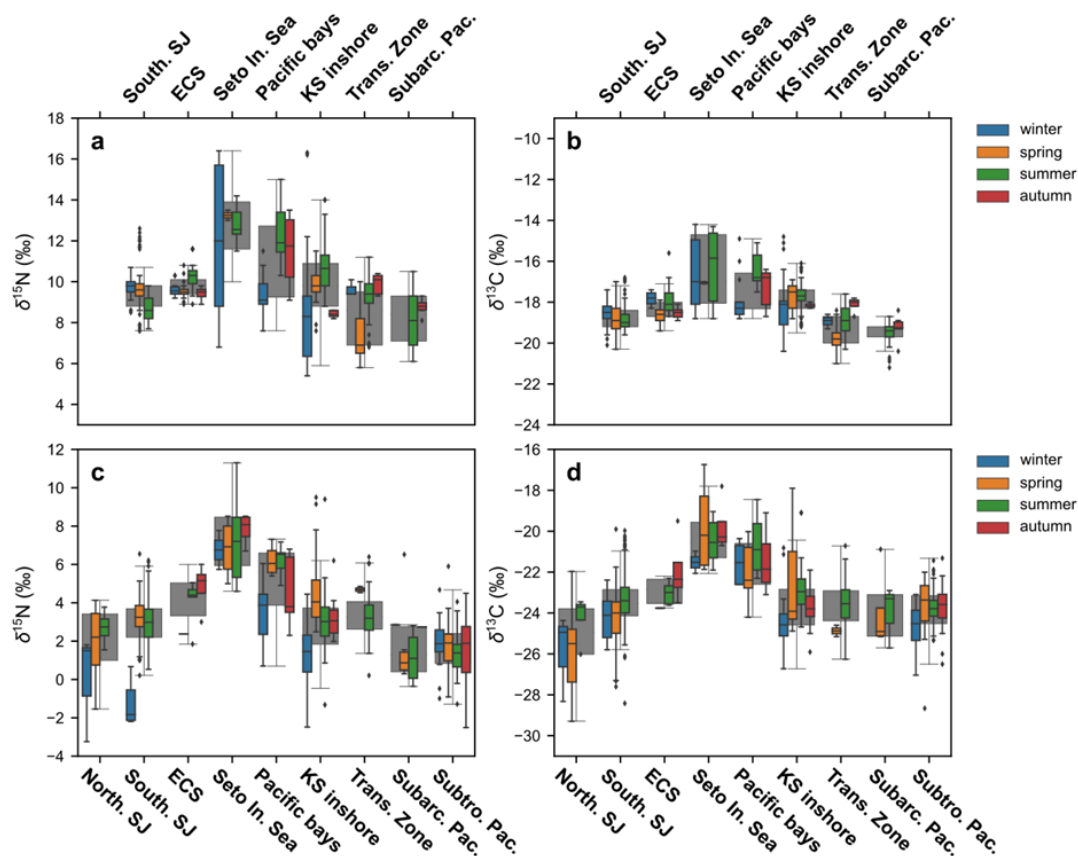
Figure 4. Differences of stable isotope ratios of sardine (a, b) and POM (c, d) among regions. Boxplots for each size season are shown for each region: center line, median; box limits, upper and lower quartiles; whiskers, 1.5x interquartile range; points, outliers. Wider grey boxplots show data distribution for each region,

433

434

435

Seasonal and geographic variations in isotopic composition POM

The total number of available data points after averaging for the same sampling date and location was 599, of which 580 were acidified to remove calcium carbonate prior to analysis (Supplementary Table 1). The number of available data varied significantly by region: over a hundred in the Southern Sea of Japan and Subtropical Pacific but only 10 in the East China Sea and 12 for the Subarctic Pacific (Supplementary Fig. 2). The δ^{15}N and δ^{13}C values of POM ranged from -4.0 to +11.3‰ with a median of +2.7 ‰ and -30.9 to -16.0‰ with a median of -23.7‰, respectively. In most regions, median δ^{15}N and δ^{13}C values of POM were lowest in winter (January to March) and higher in spring (April to June) to autumn (Fig. 4c, d). Median δ^{15}N values in each region were higher in the Seto

446   Inland Sea and Pacific Coast, moderate in the Kuroshio-Oyashio Transition Zone, East

447   China Sea, Northern and Southern Sea of Japan and Kuroshio inshore, and lower in the

448   subtropical and subarctic Pacific (Fig. 4c). Median $\delta^{13}C$ values showed similar

449   geographic patterns and were lowest in the Northern Sea of Japan (Fig. 4d).

450

451

452   *Linear model analyses*

453   To quantitatively describe the effects of fish size, seasons and regions on $\delta^{15}N$ and $\delta^{13}C$

454   of sardine, the isotope ratios were analysed using linear mixed-effects models

455   (*lmer(Sardine-$\delta^{15}N$ or -$\delta^{13}C$ ~ region + season + ln(SL) + 1|year)*). Significant effects of

456   season, region and fish size were detected (Table 1, 2). The diagnoses for the models

457   showed straight Q-Q plots and normalities and homogeneities of the residuals

458   (Supplementary Figs. 3, 4), suggesting that the models were reasonably fitted. The

459   logarithm of the standard length showed a positive effect on the $\delta^{15}N$ and $\delta^{13}C$ values

460   with a larger slope for $\delta^{15}N$ (Table 1, 2). The $\delta^{15}N$ and $\delta^{13}C$ values in summer (July to

461   September) were significantly higher than those in winter (January to March) by 1.2 ‰

462   and 0.4 ‰, respectively.

463

Table 1. Summary of the linear random-effects model (lmer(*Sardine δ¹⁵N ~ Region + season + ln(SL) + (1 | Year)*)).

Random effects:

Groups	Name	Variance	Std.Dev
Year	(Intercept)	0.21	0.46
Residual		1.87	1.37
Number of obs: 581, groups: Year, 17			

Fixed effects:

	Estimate	Std. Error	df	t value	Pr(>|t|)
(Intercept)	4.17	0.60	433.1	6.99	**1.07.E-11**
Regions Kuroshio Inshore	0.23	0.29	70.5	0.79	0.43
Regions Subarctic Pacific	-1.83	0.29	520.0	-6.24	**9.07.E-10**
Regions Pacific bays	1.44	0.32	497.8	4.53	**7.46.E-06**
Regions Seto Inland Sea	2.77	0.36	203.9	7.62	**9.55.E-13**
Regions Southern Sea of Japn	-0.17	0.20	544.0	-0.87	0.39
Regions K-O Transition Zone	-1.28	0.22	482.6	-5.78	**1.37.E-08**
ln(SL)	1.01	0.11	531.1	9.16	**< 2e-16**
Season Spring	0.73	0.20	561.0	3.71	**2.27.E-04**
Season Summer	1.21	0.19	527.4	6.46	**2.43.E-10**
Season Autumn	0.92	0.29	487.7	3.20	**1.44.E-03**

464

465

466

Table 2. Summary of the linear random-effects model (lmer(*Sardine δ¹³C ~ Region + season + ln(SL) + (1 | Year)*)).

Random effects:

Groups	Name	Variance	Std.Dev
Year	(Intercept)	0.43	0.66
Residual		0.51	0.71
Number of obs: 581, groups: Year, 17			

Fixed effects:

	Estimate	Std. Error	df	t value	Pr(>|t|)
(Intercept)	-20.38	0.35	180.4	-57.95	< 2E-16
Regions Kuroshio Inshore	0.40	0.19	406.0	2.16	3.16.E-02
Regions Subarctic Pacific	-1.41	0.16	568.7	-8.92	< 2E-16
Regions Pacific bays	0.86	0.17	568.7	5.00	7.84.E-07
Regions Seto Inland Sea	1.50	0.21	522.6	7.07	4.97.E-12
Regions Southern Sea of Japn	-0.45	0.11	569.7	-4.20	3.04.E-05
Regions K-O Transition Zone	-0.84	0.12	568.2	-6.94	1.10.E-11
ln(SL)	0.47	0.06	568.5	7.97	8.67.E-15
Season Spring	0.04	0.10	563.5	0.37	0.71
Season Summer	0.40	0.10	566.7	4.04	6.11.E-05
Season Autumn	0.19	0.16	568.7	1.24	0.22

The POM isotope ratios were also analysed using linear random-effects models *lmer(POM-δ¹⁵N or -δ¹³C ~ region + season + 1| year)*, which revealed significant effects of season and region (Supplementary Table 2, 3). Diagnoses for the models showed mostly straight Q-Q plots except for the tails, and normalities and homogeneities of residuals (Supplementary Figs. 5, 6). Seasonal trends were different for δ^{15}N and δ^{13}C: δ^{15}N was lowest in winter and highest in spring (April to June) with a difference of 1.9 ‰, while δ^{13}C was lowest in winter and highest in summer with a difference of 1.1 ‰ (Supplementary Table 4). The estimated marginal means for each region and season were compared between sardine and POM (Fig. 5a-d; Supplementary Table 4). Significant linear relationships were found using a least rectangles regression analysis assuming observational errors for both sardine and POM isotope ratios;

Sardine δ^{15}N = 1.18 × POM δ^{15}N + 5.4 (Pearson's r = 0.83, p = 0.02, n = 7)   (3),

484

485   Sardine $\delta^{13}C = 1.09 \times POM\ \delta^{13}C + 7.1$ (Pearson's r = 0.88, p = 0.008, n = 7)   (4),

486

487   where the slopes were both not significantly different from 1 ($\delta^{15}N$: t = 0.65, p = 0.54,

488    $\delta^{13}C$: t = 0.44, p = 0.68). At $\delta^{15}N$, the mean value for the Kuroshio-Oyashio Transition

489   Zone showed the largest deviation from the regression line, indicating a lower $\delta^{15}N$ of

490   sardine than that the $\delta^{15}N$ predicted by POM (Fig. 5a). Such a large deviation in the

491   Kuroshio-Oyashio Transition Zone was not observed for $\delta^{13}C$ (Fig. 5b). The magnitude

492   of seasonal variation was greater for POM than for sardine, both for $\delta^{15}N$ (sardine: ± 0.59

493   (1 SD), POM: 0.90‰) and for $\delta^{13}C$ (sardine: ± 0.22, POM: ± 0.51‰), and the highest

494   season for $\delta^{15}N$ was summer for sardine but spring for POM (Fig. 5c, d). However, when

495   the seasonal effects of POM were averaged with the previous season, the seasonal trends

496   were mostly similar to those of sardine (Fig. 5c, d).
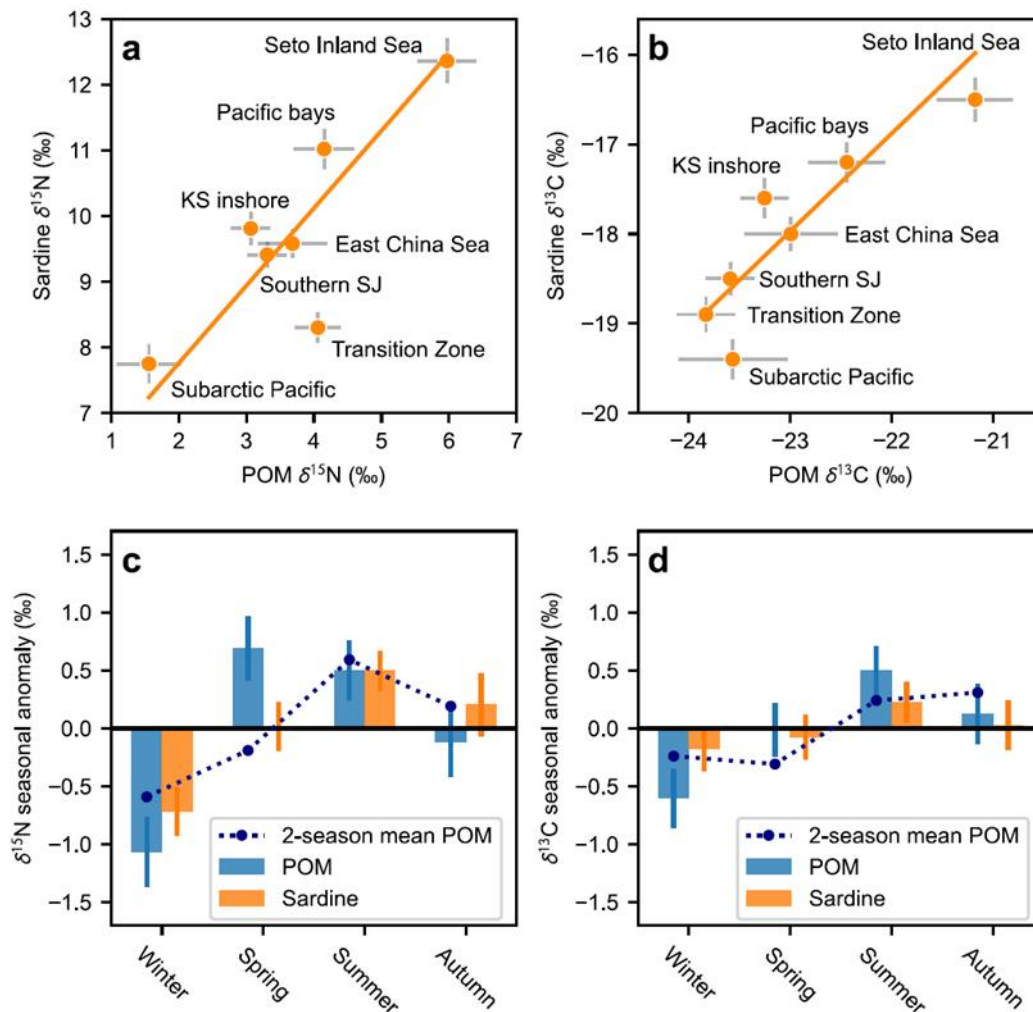
Figure 5. Comparisons of estimated marginal means of stable isotope ratios of sardine and POM for each region (a, b) and each season (c, d). Solid lines represent the linear regression lines based on a least rectangles regression analysis (a, b). The seasonal effects were shown as anomalies, and 2-season averaged effect (present and previous season) of POM are also shown (c, d). The error bars represent standard errors (a-d).

497
498
499
500 The differences in isotope ratios between POM and sardine in each region were examined
501 to find possible differences in trophic levels between the regions (Fig. 6a, b). Isotopic
502 differences between sardine and baseline ranged from 4.2‰ to 6.9‰ at δ^{15}N and from
503 3.7‰ to 5.2‰ at δ^{13}C, which tended to be greater in the Southern nearshore areas (Pacific
504 bays, Kuroshio inshore and Seto Island Sea) than in other oceanic areas (Fig. 6a, b).
505 Geographical variations in isotopic differences were mostly smaller than 1‰ in both δ^{15}N
506 and δ^{13}C, while standard errors for each isotopic difference were 0.4−0.6‰ in δ^{15}N and
507 0.3−0.6‰ in δ^{13}C. The difference in δ^{15}N between sardine and POM in the Kuroshio-

508   Oyashio Transition Zone was exceptionally low (4.2‰) compared to differences in other
509   regions, which averaged 6.4‰. However, when we calculate the δ^{15}N difference using
510   the baseline for the Subtropical Pacific (dashed bars in Fig. 6b), it is comparable to that
511   in other regions. To investigate the potential influence of Subtropical waters on larvae and
512   early juveniles collected in May 2021 in the Transition Zone, which had significantly low
513   δ^{15}N, the collection sites during a survey were compared with satellite-derived sea surface
514   height data during the survey period (Fig. 6c). The comparison showed that the δ^{15}N
515   values were particularly low near the Kuroshio Extension and the warm core rings and
516   higher away from these structures (Fig. 6c).

517
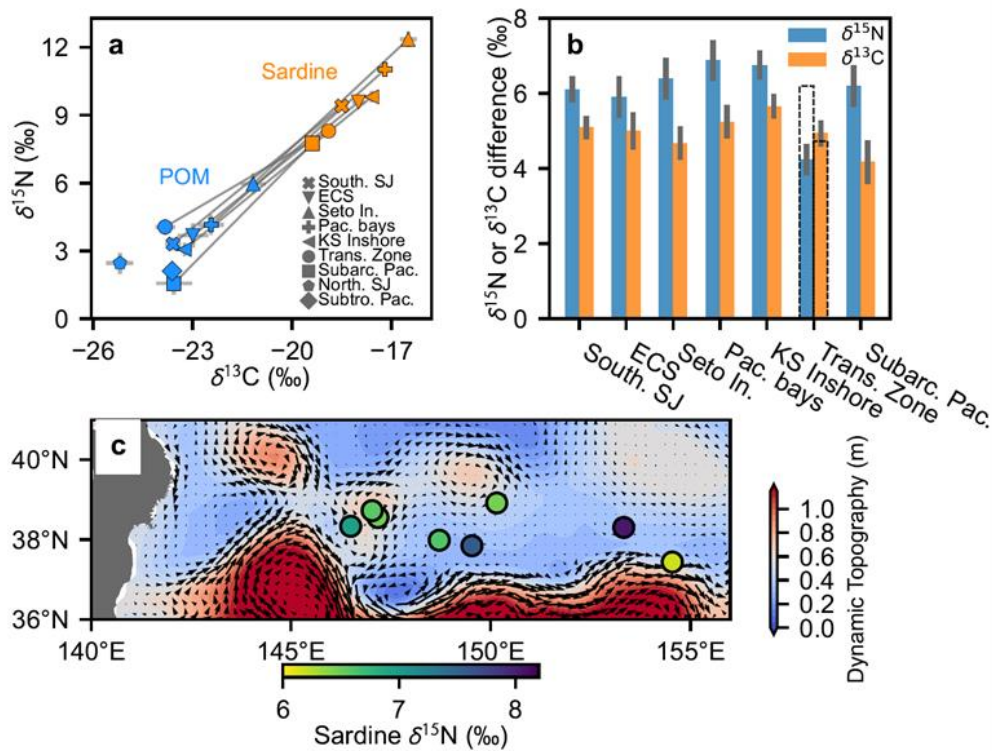
Figure 6. Differences between stable isotope ratios of POM and sardine, and potential effect of subtropical waters in the Kuroshio-Oyashio Transition Zone. The estimated marginal mean δ^{13}C and δ^{15}N for POM (blue) and sardine (orange) are plotted with different symbols for each region (a). The error bars represent standard errors (a). The differences of δ^{13}C (orange) and δ^{15}N (blue) between marginal means of sardine and POM (b). The error bars are standard errors propagated from those of sardine and POM (b). The dashed bars for the Kuroshio-Oyashio Transition Zone are the isotopic differences between sardine in the region and baseline in the Subtropical Pacific (b). Sardine δ^{15}N for samples collected during surveys in 18th to 31th May 2021 in the Transition Zone (c). Mean absolute dynamic topography and the derived surface geostrophic flow during the survey periods are shown (c).

518
519

520

521   Finally, to infer the effects of fish movements, isotope ratios of larvae and juveniles were
522   compared to the ranges of values that could be predicted from local baselines in each
523   region (Fig. 7a-l). If the isotope ratios of a fish were outside the predicted range for the
524   sampling region but within the range for the adjacent region, this may indicate that the
525   fish had recently arrived from the adjacent region. As the isotopic ratios of sardines are
526   significantly affected by fish size and seasonal and inter-annual variations, the observed
527   values were adjusted for these effects based on the results of linear mixed effects models
528   (Table 1, 2). In the Southern Sea of Japan and East China Sea, sardine isotope ratios
529   remained mostly within the local predicted ranges in each region (Fig. 7a, d, g), with the
530   exception of some larvae in the Sea of Japan (Fig. 7a) caught near an estuary (the Miho
531   Bay). While the predicted ranges for the regions overlapped, the sardines captured in the
532   local region mostly occupied the part of the predicted ranges that did not overlap (Fig. 7a,
533   d, g). In the Seto Island Sea, Pacific bays and Kuroshio inshore, sardine isotope values
534   were distributed among the predicted ranges of the lower (the Subtropical Pacific and
535   Kuroshio inshore) and higher (the Seto Inland Sea and the Pacific bays) baseline regions
536   (Fig. 7b, e, f). In the Seto Island Sea, some smaller individuals under 60 mm SL showed
537   low δ^{15}N values in the predicted ranges of the Kuroshio inshore or the Subtropical Pacific,
538   while larger individuals consistently showed higher δ^{15}N values than the ranges. In the
539   Pacific bays, sardine isotope ratios were mostly within or above the locally predicted
540   range. In the Kuroshio-Oyashio Transition Zone, smaller individuals under 60 mm SL
541   were mostly within the predicted range for the Subtropical Pacific (Fig. 7c), while larger
542   individuals tended to have higher δ^{15}N and approached the predicted range for the
543   Transition Zone (Fig. 7f, i). In the Subarctic Pacific, isotope ratios spread among the
544   predicted ranges for the Transition Zone and the Subarctic Pacific (Fig. 7i). Some
545   juveniles in the Transition Zone and Subarctic Pacific had significantly low δ^{15}N and δ^{13}C
546   values outside the predicted ranges. They were all larger than 135 mm SL and captured
547   around were caught near 175°E, except for one specimen from near 160°E
548   (Supplementary Fig. 7).

549
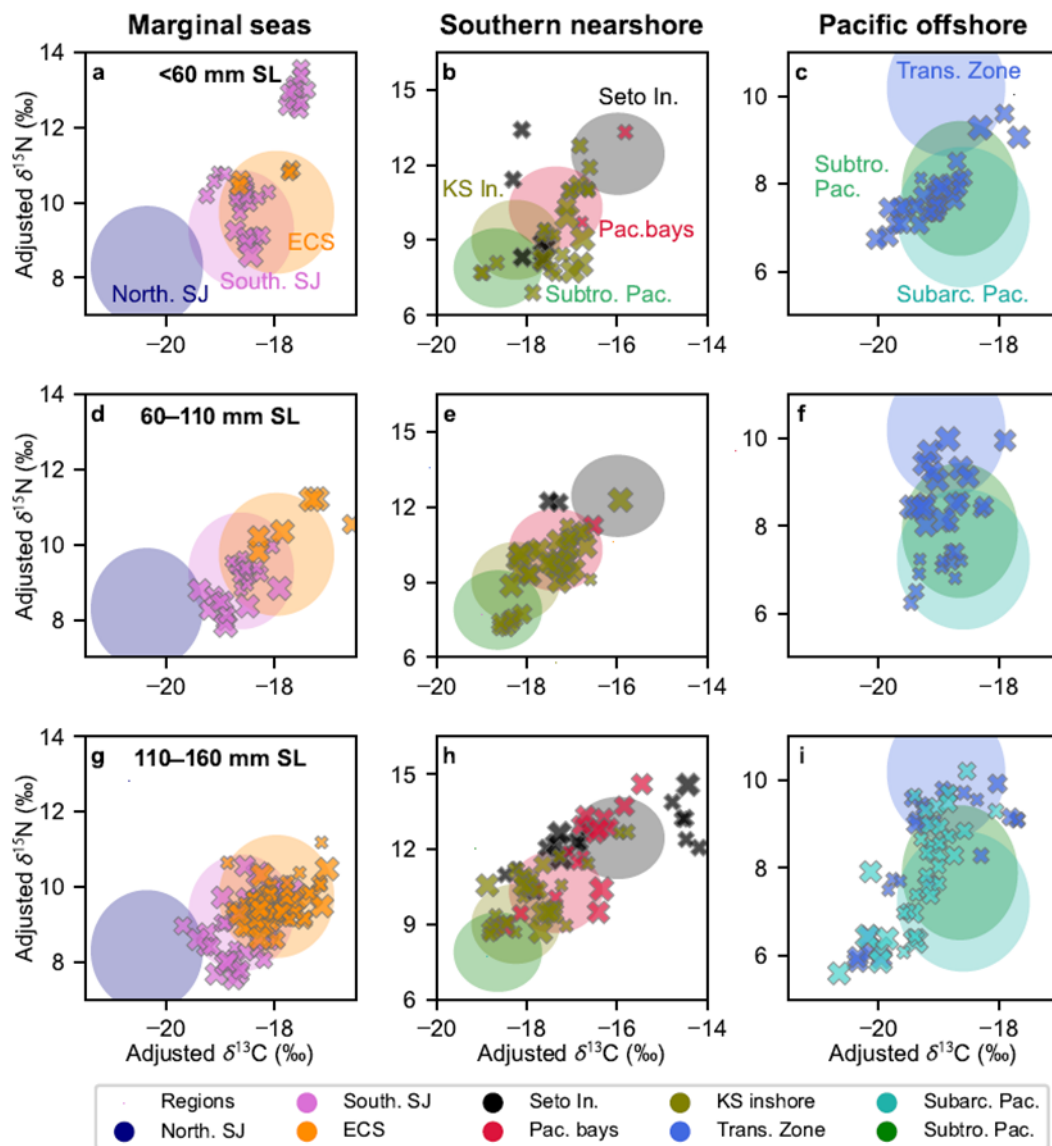
Figure 7. Comparison of the adjusted sardine $\delta^{13}C$ and $\delta^{15}N$ (x) and the predicted ranges based on local baselines (shaded). Columns represent major areas (left: the Southern Sea of Japan and East China Sea, middle: the Seto Inland Sea, Pacific bays and Kuroshio Inshore, right: the Kuroshio Oyashio Transition Zone and Subarctic Pacific), and rows represent size ranges. The sizes of the symbol for the adjusted values (x) represent the relative fish size within each size range (row), and colors represent locations at sampling.

550

551

552

Discussion

553

554   In this study, we investigated the geographic, seasonal and ontogenetic variations in $\delta^{15}N$

555   and $\delta^{13}C$ of Japanese sardine, the dominant small pelagic fish in the western North Pacific

556   and its marginal seas, and explored the mechanisms driving these variations. The $\delta^{15}N$

557   and δ^{13}C of sardine showed significant and similar geographical variations: higher in the
558   southern nearshore areas (the Seto Inland Sea, Pacific bays and Kuroshio inshore),
559   moderate in the marginal seas (the Southern Sea of Japan and the East China Sea), and
560   lower in the Pacific offshore (the Kuroshio-Oyashio Transition Zone and the Subarctic
561   Pacific). Moreover, the large geographical differences in sardine isotope ratios, up to 4‰
562   in δ^{15}N and 3‰ in δ^{13}C, were closely associated with those of POM with almost identical
563   amplitudes (Fig. 5a, b), except in the Kuroshio-Oyashio Transition Zone. Seasonal
564   differences were also found in sardine δ^{15}N and δ^{13}C values, both of which were lower in
565   winter and higher in summer. While these trends appeared to differ from those of POM,
566   they were almost identical when the effect of POM was averaged with the previous season
567   (Fig. 5c, d). This suggests that seasonal variation in POM isotope values is also reflected
568   in sardine isotope values, but in a temporally integrated manner likely due to slower
569   turnover times in organisms of higher trophic levels (Jennings et al, 2008). Geographic
570   differences in δ^{15}N and δ^{13}C between nearshore and offshore areas, or between the Pacific
571   and marginal seas have also been suggested in other small pelagic fish in the region (e.g.,
572   Japanese anchovy, Tanaka et al., 2008; Ohshimo et al., 2019). These results suggest that
573   there are significant variations in baseline isotope ratios in the western North Pacific and
574   its marginal seas, and it is the baseline variations that are mainly driving the isotopic
575   variations in small pelagic fish in the region.
576
577
578   Although the Kuroshio-Oyashio Transition Zone appeared as a significant exception in
579   the relationship between δ^{15}N of sardine and POM (Figs. 5a, 6a), this can also be
580   attributed to baseline variability. The mean δ^{15}N in sardine in the region is lowered by
581   low δ^{15}N values in spring (Fig. 3a), consisting mainly of larvae and early juveniles
582   captured in May 2021. These small individuals were captured in the southern part of the
583   Transition Zone near the Kuroshio Extension, and those closer to the Kuroshio Extension
584   and warm core rings had particularly low δ^{15}N (Fig. 6c). The baselines in the Kuroshio
585   and Kuroshio Extension that originate from the Subtropical Pacific are likely to be
586   influenced by those in the Subtropical Pacific. As the δ^{15}N baseline in the Subtropical
587   Pacific is about 2‰ lower than in the Transition Zone with comparable δ^{13}C, the observed
588   discrepancy in the δ^{15}N relationship, but not in the δ^{13}C relationship, can be explained if
589   baselines of Subtropic Pacific are simply reflected (Fig. 6b). In addition, Saino (1992)
590   found that POM δ^{15}N values are lower in a warm core ring in the Transition Zone than at
591   its periphery, possibly due to enhanced vertical mixing of the water column within the
592   ring. It is therefore likely that such local low δ^{15}N baselines near the Kuroshio Extension

593 had lowered the mean sardine δ^{15}N in the Transition Zone, which support the conclusion
594 that baseline variations are the main cause of isotopic variation in Japanese sardine.
595
596
597 The strong relationships between baselines and sardine isotope ratios indicate that mean
598 trophic levels across life stages show limited variability in its habitat. The δ^{15}N difference
599 between the marginal means of sardine and POM for each region averaged 6.4‰ with
600 less than 1‰ differences between the regions except the Transition Zone (Fig. 6b),
601 suggesting that the average trophic level of the Japanese sardine is 3.0 assuming +3.2‰
602 fractionation per trophic transfer (Sweeting et al., 2007a). Logarithmic increases in δ^{15}N
603 and δ^{13}C values with size were observed, indicating an increase in trophic level with
604 growth, particularly at early life stages (Table 1, 2). These results are consistent with
605 previous analyses of the dietary composition of Japanese sardine, which generally showed
606 that zooplankton is an important prey at most life stages, and that the size of the
607 zooplankton consumed tends to increase during growth from larval to juvenile stages
608 (Garrido and van der Lingen et al., 2009; Hirai et al., 2017; Okazaki et al., 2019). However,
609 the δ^{15}N differences between sardine and POM were slightly higher in the nearshore areas
610 (Fig. 6b), which may indicate minor dietary differences between fish in the nearshore and
611 oceanic areas. Although this remains a hypothesis given the significant uncertainty in the
612 estimates and the possible bias due to migrations (Fig. 6a, b), it is possible that nearshore
613 eutrophic areas with significant anthropogenic nutrient inputs provide larger prey for
614 sardines locally and serve as a feeding ground for a part of the population. Note that our
615 results, based on data from fish averaging 120 mm SL, do not preclude the potential
616 trophic plasticity specifically occur in adults that can heavily feed on phytoplankton by
617 filtering (Costalago et al., 2015), which should be tested in future.
618
619
620 Beyond the above trends, other notable features were observed in the isotope ratios of
621 sardine, indicating a significant influence of movements. First, the variance of δ^{15}N and
622 δ^{13}C depended on life stages, with larval and juvenile values showing significant
623 geographic variation, while adults showed less geographic variation and tended to
624 converge around the mean or extreme values. This difference likely reflects ontogenetic
625 increases in turnover time and range of movement. Isotope ratios of larvae, which have a
626 shorter turnover time (Tanaka et al., 2014), may sensitively reflect physical dynamics at
627 smaller spatial scales, as shown in the Transition Zone (Fig. 6c) or in the Southern Sea of
628 Japan (Fig. 7a), which would result in large variances. In contrast, adult isotope ratios,

629 which have longer turnover times of potentially more than several months (Bode et al.,
630 2007), may reflect spatially integrated baselines as they migrate between regions during
631 the period and absorb geographic variation. For example, the differences in δ^{15}N and δ^{13}C
632 between the Southern Sea of Japan and the East China Sea, or between the Kuroshio
633 inshore and Kuroshio-Oyashio Transition Zone, which were evident in late juveniles,
634 were no longer visible in adults (Fig. 2c, d). This suggests that the adults frequently
635 migrate between adjacent areas, as previously suspected (Kuroda, 1991). However, the
636 exceptionally high or low δ^{15}N and δ^{13}C values of some adults in the Seto Island Sea, the
637 Kuroshio inshore and Subarctic Pacific (Fig. 2d) suggest that adults can occasionally
638 remain in certain areas for months at a time. These results indicate the migratory nature
639 of the adults as well as their potential plasticity.

640
641

642 Another important feature in the isotope ratios was the different ontogenetic trends
643 between regions during the larval and juvenile stages (Fig. 3a-f). In the Southern Sea of
644 Japan and East China Sea, sardine isotope ratios did not show pronounced deviations
645 from the local predicted ranges in each region throughout the life stages (Fig. 7a, d, g),
646 suggesting that only limited or slow movements occurred. In contrast, in the Southern
647 nearshore areas, the generally large ranges of values indicate that fish frequently moved
648 between the nearshore and offshore sides, which showed a large baseline gradient (Fig.
649 7b, e, h). Larvae and early juveniles tended to have lower δ^{15}N values, suggesting that
650 many of them originate from the outer side (Fig. 7b), where the main spawning area of
651 Japanese sardine is located (Oozeki et al., 2007). In the Pacific offshore area, the increase
652 in isotope ratios with size in the Transition Zone and the wide range of values in the
653 Subarctic Pacific likely correspond to movements from the Subtropical Pacific with low
654 δ^{15}N baseline to the Transition Zone with high δ^{15}N (Fig. 7c, f, i) and from the Transition
655 Zone to the Subarctic Pacific with again low δ^{15}N (Fig. 7i), respectively. Thus, in contrast
656 to the movements in the marginal seas and southern nearshore area, systematic northward
657 movements are likely to be prevalent in the Pacific offshore, as has been previously
658 suggested by otolith isotope analysis (Sakamoto et al., 2019; 2022). The larger juveniles
659 with significantly low isotope ratios in the far offshore (Fig. 7i, Supplementary Fig. 7) are
660 probably not age-0 fish, as they were larger than 135 mm SL in the Transition Zone in
661 July. While most age-0 fish that have migrated north are considered to return to coastal
662 areas for overwintering and recruitment (Kuroda, 1991), the large juveniles may have
663 overwintered in offshore areas and therefore have low isotope ratios reflecting the
664 residual effect of lower winter baselines (Fig. 5d). These results reveal that Japanese

665 sardine exhibit remarkably different migration patterns between regions, which
666 differentially affects ontogenetic trends in isotope ratios.

667

668

669 Our results provide implications for the future use of stable isotope ratios in the western
670 North Pacific and its marginal seas. Given the considerable geographic and seasonal
671 variation in baseline and fish movements between them, the study of animal trophic
672 ecology based on bulk isotope ratios requires careful evaluation. A compound-specific
673 analysis of amino acid, which allows a clear separation of baseline and trophic effects
674 (Chikaraishi et al., 2009), is particularly recommended when geographical or seasonal
675 differences in the feeding habits of a species are to be studied, as has been done for the
676 European sardine *Sardina pilchardus* in the Mediterranean (Giménez et al., 2023).
677 Meanwhile, the geographical baseline variability in the region provides a great
678 opportunity to track the movements of animals. The strong relationship between baseline
679 and isotope ratios of sardine, which has also been demonstrated between POM and
680 myctophid fish in the Central Pacific (Horii et al., 2018), suggests the possibility of
681 modelling the isoscapes of low trophic level fishes based on baseline. Such isoscapes, in
682 combination with isotope chronology data from eye lenses or vertebrae (e.g., Wallace et
683 al, 2014; Matsubayashi et al., 2020), could be effectively used to study migratory
684 behaviours of marine predators. Systematic collection of baseline data and development
685 of models to predict baseline isoscape (e.g., Magozzi et al., 2017; St. John Glew et al.,
686 2021) would be the key for the development of this field. However, our results also show
687 that the isoscape of low trophic level fishes needs to be temporally and spatially integrated
688 from the baseline isoscape due to their migrations and slower turnover. As the spatial
689 scale of integration depends on the distance of movements during the turnover period, a
690 general understanding of the migration patterns and tissue turnover rates of small fish in
691 the region is required before the migrations of predatory fish can be studied.

692

693

694 Overall, we revealed the significant geographic, seasonal and ontogenetic variations in
695 the stable isotope ratios of Japanese sardine and comprehensively explained the
696 mechanism causing the major trends, providing insights into the ecology of the species.
697 The δ^{15}N and δ^{13}C values of Japanese sardine showed extremely large fluctuations. They
698 are primarily determined by baseline, but also influenced by differential fish movements
699 depending on life stage and region and possibly by trophic plasticity, revealing both the
700 possibility and difficulty of mechanistically predicting isotopic variability in small

pelagic fish. At least, the isotopic data and model describing the variations presented in this study may be useful in estimating the means and uncertainties of stable isotope values of sardine, which is of great ecological importance and can contribute to a better interpretation of isotopic values of variety of predators in the western North Pacific and its marginal seas.

References

A. Bode, P. Carrera, S. Lens, The pelagic foodweb in the upwelling ecosystem of Galicia (NW Spain) during spring: natural abundance of stable carbon and nitrogen isotopes. *ICES J. Mar. Sci.* **60**, 11-22 (2003).

A. Bode, M. T. Alvarez-Ossorio, M. E. Cunha, S. Garrido, J. B. Peleteiro, C. Porteiro, L. Valdés, M. Varela, Stable nitrogen isotope studies of the pelagic food web on the Atlantic shelf of the Iberian Peninsula. *Prog. Oceanogr.* **74**, 115-131 (2007).

A. Bode, P. Carrera, G. González-Nuevo, E. Nogueira, I. Riveiro, M. B. Santos, A trophic index for sardine (*Sardina pilchardus*) and its relationship to population abundance in the southern Bay of Biscay and adjacent waters of the NE Atlantic. *Prog. Oceanogr.* **166**, 139-147 (2018).

A. Brutemark, E. Lindehoff, E. Granéli, W. Granéli, Carbon isotope signature variability among cultured microalgae: influence of species, nutrients and growth. *J. Exp. Mar. Biol. Ecol.* **372**, 98-105 (2009).

J. A. Canseco, E. J. Niklitschek, C. Harrod, Variability in $\delta^{13}C$ and $\delta^{15}N$ trophic discrimination factors for teleost fishes: a meta-analysis of temperature and dietary effects. *Rev. Fish Biol. Fish.* **32**, 313–329 (2022).

L. Cardona, L. Martínez-Iñigo, R. Mateo, J. González-Solís, The role of sardine as prey for pelagic predators in the western Mediterranean Sea assessed using stable isotopes and fatty acids. *Mar. Ecol. Prog. Ser.* **531**, 1-14 (2015).

N. Chang, J. Shiao, G. Gong, S. Kao, C. Hsieh, Stable isotope ratios reveal food source of benthic fish and crustaceans along a gradient of trophic status in the East China Sea. *Cont. Shelf Res.* **84**, 23-34 (2014).

737

738   D. M. Checkley Jr, R. G. Asch, R. R. Rykaczewski, Climate, anchovy, and sardine. *Ann.*
739   *Rev. Mar. Sci.* 9, 469-493 (2017).

740

741   M. Chen, L. Guo, Q. Ma, Y. Qiu, R. Zhang, E. Lv, Y. Huang, Zonal patterns of δ^{13}C, δ^{15}N
742   and ^{210}Po in the tropical and subtropical North Pacific. *Geophys. Res. Lett.* **33**, (2006).

743

744   Y. Chikaraishi, N. O. Ogawa, Y. Kashiyama, Y. Takano, H. Suga, A. Tomitani, H.
745   Miyashita, H. Kitazato, N. Ohkouchi, Determination of aquatic food-web structure
746   based on compound-specific nitrogen isotopic composition of amino acids. *Limnol.*
747   *Oceanogr.* **7**, 740-750 (2009).

748

749   D. Costalago, S. Garrido, I. Palomera, Comparison of the feeding apparatus and diet of
750   European sardines Sardina pilchardus of Atlantic and Mediterranean waters: ecological
751   implications. *J. Fish Biol.* **86**, 1348-1362 (2015).

752

753   S. D. Costanzo, M. J. O'donohue, W. C. Dennison, N. R. Loneragan, M. Thomas, A new
754   approach for detecting and mapping sewage impacts. *Mar. Pollut. Bull.* **42**, 149-156
755   (2001).

756

757   P. M. Cury, I. L. Boyd, S. Bonhommeau, T. Anker-Nilssen, R. J. Crawford, R. W. Furness,
758   J. A. Mills, E. J. Murphy, H. Osterblom, M. Paleczny, J. F. Piatt, J. P. Roux, L. Shannon,
759   W. J. Sydeman, Global seabird response to forage fish depletion--one-third for the
760   birds. *Science.* **334**, 1703-1706 (2011).

761

762   P. M. Cury, A. Bakun, R. J. Crawford, A. Jarre, R. A. Quinones, L. J. Shannon, H. M.
763   Verheye, Small pelagics in upwelling systems: patterns of interaction and structural
764   changes in "wasp-waist" ecosystems. *ICES J. Mar. Sci.* **57**, 603-618 (2000).

765

766   M. J. DeNiro, S. Epstein, Influence of diet on the distribution of nitrogen isotopes in
767   animals. *Geochim. Cosmochim. Acta.* **45**, 341-351 (1981).

768

769   FAO. *FAO Yearbook. Fishery and Aquaculture Statistics 2019/FAO annuaire. Statistiques*
770   *des pêches et de l'aquaculture 2019/FAO anuario. Estadísticas de pesca y acuicultura*
771   *2019*. Rome/Roma (2021). https://doi.org/10.4060/cb7874t

772

773

774　K. Fukumori, M. Oi, H. Doi, N. Okuda, H. Yamaguchi, M. Kuwae, H. Miyasaka, K.
775　　　Yoshino, Y. Koizumi, K. Omori, Food sources of the pearl oyster in coastal ecosystems
776　　　of Japan: evidence from diet and stable isotope analysis. *Estuar. Coast. Shelf Sci.* **76**,
777　　　704-709 (2008).

778

779　S. Furuichi, Y. Kamimura, R. Yukami, Length–length and length–weight relationships for
780　　　four dominant small pelagic fishes in the Kuroshio–Oyashio current
781　　　system. *Thalassas.* **37**, 651-657 (2021).

782

783　S. Furuichi, T. Yasuda, H. Kurota, M. Yoda, K. Suzuki, M. Takahashi, M. Fukuwaka,
784　　　Disentangling the effects of climate and density-dependent factors on spatiotemporal
785　　　dynamics of Japanese sardine spawning. *Mar. Ecol. Prog. Ser.* **633**, 157-168 (2020).

786

787　S. Furuichi, R. Yukami, Y. Kamimura, S. Nishijima, R. Watabe, Stock assessment and
788　　　evaluation for Pacific stock of Japanese sardine (fiscal year 2021). *Marine fisheries*
789　　　*stock assessment and evaluation for Japanese waters.* Japan Fisheries Agency and
790　　　Japan Fisheries Research and Education Agency, Tokyo 50 pp (2022).
791　　　http://abchan.fra.go.jp/digests2021/index.html

792

793　S. Garrido, C. D. van der Lingen, Feeding biology and ecology. in *Biology and Ecology*
794　　　*of Sardines and Anchovies.* Edited by Konstantinos Ganias**,** CRC press, 122-189 (2014).

795

796　J. Giménez, M. Albo-Puigserver, R. Laiz-Carrión, E. Lloret-Lloret, J. M. Bellido, M. Coll,
797　　　Trophic position variability of European sardine by compound-specific stable isotope
798　　　analyses. *Can. J. Fish. Aquat. Sci.* e-First (2023).

799

800　R. Goericke, B. Fry, Variations of marine plankton $\delta13C$ with latitude, temperature, and
801　　　dissolved CO2 in the world ocean. *Global Biogeochem. Cycles.* **8**, 85-90 (1994).

802

803　N. Gruber, C. D. Keeling, R. B. Bacastow, P. R. Guenther, T. J. Lueker, M. Wahlen, H. A.
804　　　Meijer, W. G. Mook, T. F. Stocker, Spatiotemporal patterns of carbon-13 in the global
805　　　surface oceans and the oceanic Suess effect. *Global Biogeochem. Cycles.* **13**, 307-335
806　　　(1999).

807

808　C. Harrod, J. Grey, T. K. McCarthy, M. Morrissey, Stable isotope analyses provide new

809   insights into ecological plasticity in a mixohaline population of European
810   eel. *Oecologia.* **144**, 673-683 (2005).

811

812   J. Hirai, K. Hidaka, S. Nagai, T. Ichikawa, Molecular-based diet analysis of the early
813   post-larvae of Japanese sardine *Sardinops melanostictus* and Pacific round herring
814   *Etrumeus teres. Mar. Ecol. Prog. Ser.* **564**, 99-113 (2017).

815

816   P. Ho, N. Okuda, C. Yeh, P. Wang, G. Gong, C. Hsieh, Carbon and nitrogen isoscape of
817   particulate organic matter in the East China Sea. *Prog. Oceanogr.* **197**, 102667 (2021).

818

819   S. Horii, K. Takahashi, T. Shiozaki, F. Hashihama, K. Furuya, Stable isotopic evidence
820   for the differential contribution of diazotrophs to the epipelagic grazing food chain in
821   the mid-Pacific Ocean. *Global Ecol. Biogeogr.* **27**, 1467-1480 (2018).

822

823   A. Hoshika, M. J. Sarker, S. Ishida, Y. Mishima, N. Takai, Food web analysis of an
824   eelgrass (*Zostera marina* L.) meadow and neighbouring sites in Mitsukuchi Bay (Seto
825   Inland Sea, Japan) using carbon and nitrogen stable isotope ratios. *Aquat. Bot.* **85**, 191-
826   197 (2006).

827

828   M. Inoue, Y. Shirotani, T. Morokado, S. Hanaki, M. Ito, H. Kameyama, H. Kofuji, A.
829   Okino, T. Shikata, M. Yoshida, Kuroshio fractions in the southwestern sea of Japan;
830   implications from radium isotopes. *Cont. Shelf Res.* **214**, 104328 (2021).

831

832   O. Isoguchi, H. Kawamura, E. Oka, Quasi-stationary jets transporting surface warm
833   waters across the transition zone between the subtropical and the subarctic gyres in the
834   North Pacific. *J. Geophys. Res. Oceans* **111**, (2006).

835

836   S. Itoh, I. Yasuda, H. Nishikawa, H. Sasaki, Y. Sasai, Transport and environmental
837   temperature variability of eggs and larvae of the Japanese anchovy (*Engraulis
838   japonicus*) and Japanese sardine (*Sardinops melanostictus*) in the western North Pacific
839   estimated via numerical particle-tracking experiments. *Fish. Oceanogr.* **18**, 118-133
840   (2009).

841

842   S. Itoh, I. Yasuda, Characteristics of mesoscale eddies in the Kuroshio–Oyashio Extension
843   region detected from the distribution of the sea surface height anomaly. *J. Phys.
844   Oceanogr.* **40**, 1018-1034 (2010).

845

846 S. Jennings, T. A. Maxwell, M. Schratzberger, S. P. Milligan, Body-size dependent
847   temporal variations in nitrogen stable isotope ratios in food webs. *Mar. Ecol. Prog.*
848   *Ser.* **370**, 199-206 (2008).

849

850 A. Kasai, H. Horie, W. Sakamoto, Selection of food sources by *Ruditapes philippinarum*
851   and *Mactra veneriformis* (Bivalva: Mollusca) determined from stable isotope
852   analysis. *Fish. Sci.* **70**, 11-20 (2004).

853

854 T. Kodama, A. Nishimoto, S. Horii, D. Ito, T. Yamaguchi, K. Hidaka, T. Setou, T. Ono,
855   Spatial and seasonal variations of stable isotope ratios of particulate organic carbon and
856   nitrogen in the surface water of the Kuroshio. *J. Geophys. Res. Oceans.* **126**,
857   e2021JC017175 (2021).

858

859 T. Kodama, Y. Igeta, N. Iguchi, Long-Term Variation in mesozooplankton biomass caused
860   by top-down effects: a case study in the coastal sea of Japan. *Geophys. Res. Lett.* **49**,
861   e2022GL099037 (2022a).

862

863 T. Kodama, A. Nishimoto, K. Nakamura, M. Nakae, N. Iguchi, Y. Igeta, Y. Kogure,
864   Variations in the ratio of carbon and nitrogen stable isotopes of particulate organic
865   matter in the southern Sea of Japan. *ESS Open Archive*, (2022b).
866   DOI: 10.1002/essoar.10512108.1

867

868 C. M. Kurle, J. K. McWhorter, Spatial and temporal variability within marine isoscapes:
869   implications for interpreting stable isotope data from marine systems. *Mar. Ecol. Prog.*
870   *Ser.* **568**, 31-45 (2017).

871

872 K. Kuroda, Studies on the recruitment process focusing on the early life history of the
873   Japanese sardine, *Sardinops melanostictus* (Schlegel). *Bull. Natl. Res. Inst. Fish. Sci.* **3**,
874   25-278 (1991).

875

876 A. Kuznetsova, P. B. Brockhoff, R. H. B. Christensen, lmerTest Package: Tests in Linear
877   Mixed Effects Models. *J. Stat. Soft.* **82**, 1 (2017).

878

879 R. V. Lenth, emmeans: Estimated Marginal Means, aka Least-Squares Means. R package
880   version 1.7.5. (2022). https://CRAN.R-project.org/package=emmeans

881

882 D. J. Lindsay, M. Minagawa, I. Mitani, K. Kawaguchi, Trophic shift in the Japanese
883   anchovy *Engraulis japonicus* in its early life history stages as detected by stable isotope
884   ratios in Sagami Bay, Central Japan. *Fish. Sci.* **64**, 403-410 (1998).

885

886 K. Liu, M. Su, C. Hsueh, G. Gong, The nitrogen isotopic composition of nitrate in the
887   Kuroshio Water northeast of Taiwan: Evidence for nitrogen fixation as a source of
888   isotopically light nitrate. *Mar. Chem.* **54**, 273-292 (1996).

889

890 S. Magozzi, A. Yool, H. B. Vander Zanden, M. B. Wunder, C. N. Trueman, Using ocean
891   models to predict spatial and temporal variation in marine carbon
892   isotopes. *Ecosphere.* **8**, e01763 (2017).

893

894 W. Mei, Feeding Habit Analysis of Early Life Fishes in the East China Sea, Based on
895   Ultra-Sensitive Stable Isotopes Analyses. *Doctoral dissertation, school of fisheries*
896   *science and environmental studies, Nagasaki University,* pp 161, (2018).

897

898 J. Matsubayashi, Y. Osada, K. Tadokoro, Y. Abe, A. Yamaguchi, K. Shirai, K. Honda, C.
899   Yoshikawa, N. O. Ogawa, N. Ohkouchi, Tracking long-distance migration of marine
900   fishes using compound-specific stable isotope analysis of amino acids. *Ecol. Lett.* **23**,
901   881-890 (2020).

902

903 T. W. Miller, K. Omori, H. Hamaoka, J. Shibata, O. Hidejiro, Tracing anthropogenic
904   inputs to production in the Seto Inland Sea, Japan–A stable isotope approach. *Mar.*
905   *Pollut. Bull.* **60**, 1803-1809 (2010).

906

907 M. Minagawa, M. Ohashi, T. Kuramoto, N. Noda, δ^{15}N of PON and nitrate as a clue to
908   the origin and transformation of nitrogen in the subarctic North Pacific and its marginal
909   sea. *J. Oceanogr.* **57**, 285-300 (2001).

910

911 M. Minagawa, E. Wada, Stepwise enrichment of ^{15}N along food chains: further evidence
912   and the relation between δ^{15}N and animal age. *Geochim. Cosmochim. Acta.* **48**, 1135-
913   1140 (1984).

914

915 Y. Mino, C. Sukigara, M. C. Honda, H. Kawakami, M. Wakita, K. Sasaoka, C. Yoshikawa,
916   O. Abe, J. Kaiser, K. Kimoto, Seasonal and interannual variations in nitrogen

availability and particle export in the northwestern North Pacific subtropical gyre. *J. Geophys. Res. Oceans.* **125**, e2019JC015600 (2020).

Y. Mino, C. Sukigara, M. C. Honda, H. Kawakami, K. Matsumoto, M. Wakita, M. Kitamura, T. Fujiki, K. Sasaoka, O. Abe, Seasonal variations in the nitrogen isotopic composition of settling particles at station K2 in the western subarctic North Pacific. *J. Oceanogr.* **72**, 819-836 (2016).

S. Moriyasu, The Tsushima Current. In, *Kuroshio Its Physical Aspects*, edited by H. Stommel, K. Yoshida. University of Tokyo Press, Tokyo, 353-369 (1972).

S. Muko, S. Ohshimo, H. Kurota, T. Yasuda, M. Fukuwaka, Long-term change in the distribution of Japanese sardine in the Sea of Japan during population fluctuations. *Mar. Ecol. Prog. Ser.* **593**, 141-154 (2018).

S. Nakai, Y. Soga, S. Sekito, A. Umehara, T. Okuda, M. Ohno, W. Nishijima, S. Asaoka, Historical changes in primary production in the Seto Inland Sea, Japan, after implementing regulations to control the pollutant loads. *Water Policy.* **20**, 855-870 (2018).

K. Nakamura, A. Nishimoto, S. Yasui-Tamura, Y. Kogure, M. Nakae, N. Iguchi, H. Morimoto, T. Kodama, Carbon and nitrogen dynamics in the coastal Sea of Japan inferred from 15 years of measurements of stable isotope ratios of *Calanus sinicus*. *Ocean Science.* **18**, 295-305 (2022).

H. Nakano, H. Tsujino, K. Sakamoto, S. Urakawa, T. Toyoda, G. Yamanaka, Identification of the fronts from the Kuroshio Extension to the Subarctic Current using absolute dynamic topographies in satellite altimetry products. *J. Oceanogr.* **74**, 393-420 (2018).

Y. Niino, S. Furuichi, Y. Kamimura, R. Yukami, Spatiotemporal spawning patterns and early growth of Japanese sardine in the western North Pacific during the recent stock increase. *Fish. Oceanogr.* **30**, 643-652 (2021).

S. Ohshimo, T. Kodama, T. Yasuda, S. Kitajima, T. Tsuji, H. Kidokoro, H. Tanaka, Potential fluctuation of $\delta^{13}C$ and $\delta^{15}N$ values of small pelagic forage fish in the Sea of Japan and East China Sea. *Mar. Freshw. Res.* **72**, 1811-1823 (2021).

953

954 S. Ohshimo, D. J. Madigan, T. Kodama, H. Tanaka, K. Komoto, S. Suyama, T. Ono, T.
955 Yamakawa, Isoscapes reveal patterns of δ^{13}C and δ^{15}N of pelagic forage fish and squid
956 in the Northwest Pacific Ocean. *Prog. Oceanogr.* **175**, 124-138 (2019).

957

958 Y. Okazaki, K. Tadokoro, H. Kubota, Y. Kamimura, K. Hidaka, Dietary overlap and
959 optimal prey environments of larval and juvenile sardine and anchovy in the mixed
960 water region of the western North Pacific. *Mar. Ecol. Prog. Ser.* **630**, 149-160 (2019).

961

962 Y. Oozeki, A. Takasuka, H. Kubota, M. Barange, Characterizing Spawning Habitats of
963 Japanese Sardine, *Sardinops Melanostictus*, Japanese Anchovy, *Engraulis Japonicus*,
964 and Pacific Round Herring, *Etrumeus teres*, in the Northwestern Pacific. *CalCOFI*
965 *Rep.* **48**, 191 (2007).

966

967 H. Pethybridge, C. A. Choy, J. M. Logan, V. Allain, A. Lorrain, N. Bodin, C. J. Somes, J.
968 Young, F. Ménard, C. Langlais, A global meta-analysis of marine predator nitrogen
969 stable isotopes: Relationships between trophic structure and environmental
970 conditions. *Global Ecol. Biogeogr.* **27**, 1043-1055 (2018).

971

972 D. L. Phillips, R. Inger, S. Bearhop, A. L. Jackson, J. W. Moore, A. C. Parnell, B. X.
973 Semmens, E. J. Ward, Best practices for use of stable isotope mixing models in food-
974 web studies. *Can. J. Zool.* **92**, 823-835 (2014).

975

976 R Core Team, R: A language and environment for statistical computing. R Foundation for
977 Statistical Computing, Vienna, Austria (2022). URL https://www.R-project.org/.

978

979 G. H. Rau, C. Low, J. T. Pennington, K. R. Buck, F. P. Chavez, Suspended particulate
980 nitrogen δ^{15}N versus nitrate utilization: observations in Monterey Bay, CA. *Deep Sea*
981 *Res. Part II Top. Stud. Oceanogr.* **45**, 1603-1616 (1998).

982

983 T. M. Richards, T. T. Sutton, R. D. Wells, Trophic structure and sources of variation
984 influencing the stable isotope signatures of meso-and bathypelagic micronekton
985 fishes. *Front. Mar. Sci.* **7**, 507992 (2020).

986

987 T. Saino, ^{15}N and ^{13}C natural abundance in suspended particulate organic matter from a
988 Kuroshio warm-core ring. *Deep Sea Research Part A. Oceanographic Research*

989   *Papers.* **39**, S347-S362 (1992).

991   H. Saito, A. Tsuda, H. Kasai, Nutrient and plankton dynamics in the Oyashio region of
992   the western subarctic. *Deep Sea Res. Part II Top. Stud. Oceanogr.* **49**, 5463-5486
993   (2002).

995   T. Sakamoto, K. Komatsu, K. Shirai, T. Higuchi, T. Ishimura, T. Setou, Y. Kamimura, C.
996   Watanabe, A. Kawabata, Combining microvolume isotope analysis and numerical
997   simulation to reproduce fish migration history. *Methods Ecol. Evol.* **10**, 59-69 (2019).

999   T. Sakamoto, M. Takahashi, M. Chung, R. R. Rykaczewski, K. Komatsu, K. Shirai, T.
1000   Ishimura, T. Higuchi, Contrasting life-history responses to climate variability in eastern
1001   and western North Pacific sardine populations. *Nat. Commun.* **13**, 5298 (2022).

1003   M. Sano, K. Maki, Y. Nishibe, T. Nagata, S. Nishida, Feeding habits of mesopelagic
1004   copepods in Sagami Bay: insights from integrative analysis. *Prog. Oceanogr.* **110**, 11-
1005   26 (2013).

1007   P. E. Smith, Life-stage duration and survival parameters as related to interdecadal
1008   population variability in Pacific sardine. *CalCOFI Rep.* **33**, 41-47 (1992).

1010   K. St John Glew, B. Espinasse, B. P. Hunt, E. A. Pakhomov, S. J. Bury, M. Pinkerton, S.
1011   D. Nodder, A. Gutiérrez-Rodríguez, K. Safi, J. C. Brown, Isoscape models of the
1012   Southern Ocean: Predicting spatial and temporal variability in carbon and nitrogen
1013   isotope compositions of particulate organic matter. *Global Biogeochem. Cycles.* **35**,
1014   e2020GB006901 (2021).

1016   C. J. Sweeting, J. Barry, C. Barnes, N. Polunin, S. Jennings, Effects of body size and
1017   environment on diet-tissue δ^{15}N fractionation in fishes. *J. Exp. Mar. Biol. Ecol.* **340**, 1-
1018   10 (2007a).

1020   C. J. Sweeting, J. T. Barry, N. V. C. Polunin, S. Jennings, Effects of body size and
1021   environment on diet-tissue δ^{13}C fractionation in fishes. *J. Exp. Mar. Biol. Ecol.* **352**,
1022   165-176 (2007b).

1024   M. Takahashi, T. Tamura, T. Bando, K. Konishi, Feeding habits of Bryde's and sei whales

1025   in the western North Pacific inferred from stomach contents and skin stable isotope
1026   ratios. *J. Sea Res.* **184**, 102204 (2022).

1028 N. Takai, N. Hirose, T. Osawa, K. Hagiwara, T. Kojima, Y. Okazaki, T. Kuwae, T.
1029   Taniuchi, K. Yoshihara, Carbon source and trophic position of pelagic fish in coastal
1030   waters of south-eastern Izu Peninsula, Japan, identified by stable isotope analysis. *Fish.*
1031   *Sci.* **73**, 593-608 (2007).

1033 N. Takai, Y. Mishima, A. Yorozu, A. Hoshika, Carbon sources for demersal fish in the
1034   western Seto Inland Sea, Japan, examined by δ^{13}C and δ^{15}N analyses. *Limnol.*
1035   *Oceanogr.* **47**, 730-741 (2002).

1037 H. Takeoka, Progress in Seto Inland sea research. *J. Oceanogr.* **58**, 93-107 (2002).

1039 H. Tanaka, A. Takasuka, I. Aoki, S. Ohshimo, Geographical variations in the trophic
1040   ecology of Japanese anchovy, *Engraulis japonicus,* inferred from carbon and nitrogen
1041   stable isotope ratios. *Mar. Biol.* **154**, 557-568 (2008).

1043 Y. Tanaka, H. Minami, Y. Ishihi, K. Kumon, K. Higuchi, T. Eba, A. Nishi, H. Nikaido, S.
1044   Shiozawa, Relationship between prey utilization and growth variation in hatchery-
1045   reared Pacific bluefin tuna, *Thunnus orientalis* (Temminck et Schlegel), larvae
1046   estimated using nitrogen stable isotope analysis. *Aquac Res.* **45**, 537-545 (2014).

1048 P. R. Teske, A. Emami-Khoyi, T. R. Golla, J. Sandoval-Castillo, T. Lamont, B. Chiazzari,
1049   C. D. McQuaid, L. B. Beheregaray, C. D. van der Lingen, The sardine run in
1050   southeastern Africa is a mass migration into an ecological trap. *Sci. Adv.* **7**, eabf4514
1051   (2021).

1053 M. Toyokawa, T. Toda, T. Kikuchi, H. Miyake, J. Hashimoto, Direct observations of a
1054   dense occurrence of *Bolinopsis infundibulum* (Ctenophora) near the seafloor under the
1055   Oyashio and notes on their feeding behavior. *Deep Sea Res. Part I Oceanogr.* **50**, 809-
1056   813 (2003).

1058 C. N. Trueman, A. L. Jackson, K. S. Chadwick, E. J. Coombs, L. J. Feyrer, S. Magozzi,
1059   R. C. Sabin, N. Cooper, Combining simulation modeling and stable isotope analyses
1060   to reconstruct the last known movements of one of Nature's giants. *PeerJ.* **7**, e7912

1061   (2019).

1063   A. Y. Velikanov, Pacific sardine *(Sardinops melanostictus*) migrations to the shores of
1064   Sakhalin Island in the 20th–early 21st centuries. *J. Ichthyol.* **56**, 715-727 (2016).

1066   M. Voss, J. W. Dippner, J. P. Montoya, Nitrogen isotope patterns in the oxygen-deficient
1067   waters of the Eastern Tropical North Pacific Ocean. *Deep Sea Res. Part I Oceanogr.* **48**,
1068   1905-1921 (2001).

1070   A. A. Wallace, D. J. Hollander, E. B. Peebles, Stable isotopes in fish eye lenses as
1071   potential recorders of trophic and geographic history. *PLoS One.* **9**, e108935 (2014).

1073   Y. Wu, J. Zhang, D. J. Li, H. Wei, R. X. Lu, Isotope variability of particulate organic
1074   matter at the PN section in the East China Sea. *Biogeochemistry.* **65**, 31-49 (2003).

1076   I. Yabe, Y. Kawaguchi, T. Wagawa, S. Fujio, Anatomical study of Tsushima Warm Current
1077   system: determination of principal pathways and its variation. *Prog. Oceanogr.* **194**,
1078   102590 (2021).

1080   H. Yamaguchi, N. Takai, M. Ueno, I. Hayashi, Changes of the trophic position of the
1081   Japanese flounder *Paralichthys olivaceus* juvenile in a sandy sublittoral area in Wakasa
1082   Bay, Sea of Japan, examined by carbon and nitrogen isotope analyses. *Fish. Sci.* **72**,
1083   449-451 (2006).

1085   M. Yamamoto, S. Katayama, Interspecific comparisons of feeding habit between
1086   Japanese anchovy Engraulis japonicus and Japanese sardine Sardinops melanostictus
1087   in eastern Hiuchi-nada, central Seto Inland Sea, Japan, in 1995. *Bull. Jpn. Soc. Fish.*
1088   *Oceanogr.* **76**, 66-76 (2012).

1090   I. Yasuda, Hydrographic structure and variability in the Kuroshio-Oyashio transition
1091   area. *J. Oceanogr.* **59**, 389-402 (2003).

1093   N. Yasue, R. Doiuchi, A. Takasuka, Trophodynamic similarities of three sympatric
1094   clupeoid species throughout their life histories in the Kii Channel as revealed by stable
1095   isotope approach. *ICES J. Mar. Sci.* **71**, 44-55 (2014).

1097 H. Yokoyama, Y. Ishihi, Feeding of the bivalve *Theora lubrica* on benthic microalgae:
1098   isotopic evidence. *Mar. Ecol. Prog. Ser.* **255**, 303-309 (2003).
1099
1100 Z. Zhou, R. Yu, C. Sun, M. Feng, M. Zhou, Impacts of Changjiang River discharge and
1101   Kuroshio intrusion on the diatom and dinoflagellate blooms in the East China
1102   Sea. *Deep Sea Res. Part I Oceanogr.* **124**, 5244-5257 (2019).
1103

Data and Code Availability
The newly obtained isotope data of sardine and analysing codes will be deposited when accepted.

Author Contributions
Tatsuya Sakamoto: Conceptualization, Methodology, Software, Validation, Formal analysis, Investigation, Resources, Data Curation, Writing- Original draft, Visualisation. **Taketoshi Kodama:** Methodology, Data curation, Investigation, Resources, Writing- Reviewing and Editing. **Sachiko Horii:** Data curation, Resources, Investigation, Writing- Reviewing and Editing, Visualisation. **Kazutaka Takahashi:** Resources, Writing- Reviewing and Editing. **Atsushi Tawa:** Writing- Reviewing and Editing. **Yosuke Tanaka**: Writing- Reviewing and Editing, Project administration. **Seiji Ohshimo:** Resources, Writing- Reviewing and Editing, Project administration.